Astronomy & Astrophysics manuscript no. output
May 7, 2026

Euclid preparation

XCVII. Cosmology Likelihood for Observables in Euclid (CLOE). 4: Validation and performance

Euclid Collaboration: M. Martinelli[⋆1,2], A. Pezzotta[3,4], D. Sciotti[1,2], L. Blot[5,6], M. Bonici[7,8], S. Camera[9,10,11], G. Cañas-Herrera[12,13,14], V. F. Cardone[1,2], P. Carrilho[15], S. Casas[16], S. Davini[17], S. Di Domizio[18,17], S. Farrens[19], L. W. K. Goh[19], S. Gouyou Beauchamps[20,21], S. Ilić[22,23], S. Joudaki[24,25], F. Keil[23], A. M. C. Le Brun[26], C. Moretti[27,28,29,30,31], V. Pettorino[12], A. G. Sánchez[4], Z. Sakr[32,23,33], K. Tanidis[34], I. Tutusaus[23], V. Ajani[19,35,36], M. Crocce[21,20], C. Giocoli[37,38], L. Legrand[39,40], M. Lembo[41,42], G. F. Lesci[43,37], D. Navarro-Gironés[14], A. Nouri-Zonoz[44], S. Pamuk[45], M. Tsedrik[15,46], J. Bel[47], C. Carbone[7], C. A. J. Duncan[48], M. Kilbinger[19], F. Lacasa[49,50], M. Lattanzi[42], D. Sapone[51], E. Sellentin[52,14], P. L. Taylor[53,54], N. Aghanim[50], B. Altieri[55], L. Amendola[32], S. Andreon[3], N. Auricchio[37], C. Baccigalupi[30,29,31,27], M. Baldi[56,37,38], A. Balestra[57], S. Bardelli[37], P. Battaglia[37], R. Bender[4,58], A. Biviano[29,30], A. Bonchi[59], D. Bonino[11], E. Branchini[18,17,3], M. Brescia[60,61], J. Brinchmann[62,63], V. Capobianco[11], J. Carretero[24,64], M. Castellano[1], G. Castignani[37], S. Cavuoti[61,65], K. C. Chambers[66], A. Cimatti[67], C. Colodro-Conde[68], G. Congedo[15], C. J. Conselice[48], L. Conversi[69,55], Y. Copin[70], H. M. Courtois[71], A. Da Silva[72,73], H. Degaudenzi[74], S. de la Torre[75], G. De Lucia[29], A. M. Di Giorgio[76], H. Dole[50], F. Dubath[74], X. Dupac[55], S. Dusini[77], A. Ealet[70], S. Escoffier[78], M. Farina[76], R. Farinelli[37], F. Faustini[59,1], S. Ferriol[70], F. Finelli[37,79], P. Fosalba[20,21], S. Fotopoulou[80], N. Fourmanoit[78], M. Frailis[29], E. Franceschi[37], M. Fumana[7], S. Galeotta[29], K. George[58], W. Gillard[78], B. Gillis[15], J. Gracia-Carpio[4], B. R. Granett[3], A. Grazian[57], F. Grupp[4,58], L. Guzzo[81,3,82], S. V. H. Haugan[83], H. Hoekstra[14], W. Holmes[84], F. Hormuth[85], A. Hornstrup[86,87], P. Hudelot[88], K. Jahnke[89], M. Jhabvala[90], B. Joachimi[91], E. Keihänen[92], S. Kermiche[78], A. Kiessling[84], B. Kubik[70], K. Kuijken[14], M. Kümmel[58], M. Kunz[44], H. Kurki-Suonio[93,94], P. Liebing[95], S. Ligori[11], P. B. Lilje[83], V. Lindholm[93,94], I. Lloro[96], G. Mainetti[97], D. Maino[81,7,82], E. Maiorano[37], O. Mansutti[29], S. Marcin[98], O. Marggraf[99], K. Markovic[84], N. Martinet[75], F. Marulli[43,37,38], R. Massey[100], S. Maurogordato[101], E. Medinaceli[37], S. Mei[102,103], Y. Mellier[104,88], M. Meneghetti[37,38], E. Merlin[1], G. Meylan[105], A. Mora[106], M. Moresco[43,37], L. Moscardini[43,37,38], C. Neissner[107,64], S.-M. Niemi[12], J. W. Nightingale[108], C. Padilla[107], S. Paltani[74], F. Pasian[29], K. Pedersen[109], W. J. Percival[8,110,111], S. Pires[19], G. Polenta[59], M. Poncet[112], L. A. Popa[113], F. Raison[4], R. Rebolo[68,114,115], A. Renzi[116,77], J. Rhodes[84], G. Riccio[61], E. Romelli[29], M. Roncarelli[37], R. Saglia[58,4], B. Sartoris[58,29], J. A. Schewtschenko[15], P. Schneider[99], T. Schrabback[117], A. Secroun[78], E. Sefusatti[29,30,31], G. Seidel[89], M. Seiffert[84], S. Serrano[20,118,21], P. Simon[99], C. Sirignano[116,77], G. Sirri[38], A. Spurio Mancini[119], L. Stanco[77], J. Steinwagner[4], P. Tallada-Crespí[24,64], D. Tavagnacco[29], A. N. Taylor[15], I. Tereno[72,120], S. Toft[121,122], R. Toledo-Moreo[123], F. Torradeflot[64,24], L. Valenziano[37,79], J. Valiviita[93,94], T. Vassallo[58,29], G. Verdoes Kleijn[124], A. Veropalumbo[3,17,18], Y. Wang[125], J. Weller[58,4], G. Zamorani[37], F. M. Zerbi[3], E. Zucca[37], V. Allevato[61], M. Ballardini[41,42,37], M. Bolzonella[37], E. Bozzo[74], C. Burigana[126,79], R. Cabanac[23], M. Calabrese[127,7], D. Di Ferdinando[38], J. A. Escartin Vigo[4], L. Gabarra[34], J. Martín-Fleitas[106], S. Matthew[15], N. Mauri[67,38], R. B. Metcalf[43,37], M. Pöntinen[93], C. Porciani[99], I. Risso[128], V. Scottez[104,129], M. Sereno[37,38], M. Tenti[38], M. Viel[30,29,27,31,28], M. Wiesmann[83], Y. Akrami[130,131], S. Alvi[41], I. T. Andika[132,133], R. E. Angulo[134,135], S. Anselmi[77,116,6], M. Archidiacono[81,82], F. Atrio-Barandela[136], A. Balaguera-Antolinez[68], M. Bethermin[137], A. Blanchard[23], H. Böhringer[4,138,139], S. Borgani[140,30,29,31,28], M. L. Brown[48], S. Bruton[141], A. Calabro[1], B. Camacho Quevedo[20,21], A. Cappi[37,101], F. Caro[1], C. S. Carvalho[120], T. Castro[29,31,30,28], F. Cogato[43,37], S. Conseil[70], A. R. Cooray[142], O. Cucciati[37], F. De Paolis[143,144,145], G. Desprez[124], A. Díaz-Sánchez[146], J. J. Diaz[68], J. M. Diego[45], P. Dimauro[1,147], A. Enia[56,37], Y. Fang[58], A. G. Ferrari[38], P. G. Ferreira[34], A. Finoguenov[93], A. Fontana[1], A. Franco[144,143,145], K. Ganga[102], J. García-Bellido[130], T. Gasparetto[29], V. Gautard[148], R. Gavazzi[75,88], E. Gaztanaga[21,20,25], F. Giacomini[38], F. Gianotti[37], G. Gozaliasl[149,93], A. Gruppuso[37,38], M. Guidi[56,37], C. M. Gutierrez[150], A. Hall[15], S. Hemmati[151], H. Hildebrandt[152], J. Hjorth[109], J. J. E. Kajava[153,154], Y. Kang[74], V. Kansal[155,156],

Article published by EDP Sciences, to be cited as https://doi.org/10.1051/0004-6361/202556864

D. Karagiannis[41,157], K. Kiiveri[92], C. C. Kirkpatrick[92], S. Kruk[55], J. Le Graet[78], F. Lepori[158], G. Leroy[159,100], J. Lesgourgues[16], L. Leuzzi[43,37], T. I. Liaudat[160], S. J. Liu[76], A. Loureiro[161,162], J. Macias-Perez[163], G. Maggio[29], M. Magliocchetti[76], F. Mannucci[164], R. Maoli[165,1], C. J. A. P. Martins[166,62], L. Maurin[50], M. Migliaccio[167,168], M. Miluzio[55,169], P. Monaco[140,29,31,30], G. Morgante[37], S. Nadathur[25], K. Naidoo[25], P. Natoli[41,42], A. Navarro-Alsina[99], S. Nesseris[130], L. Pagano[41,42], F. Passalacqua[116,77], K. Paterson[89], L. Patrizii[38], A. Pisani[78,170], D. Potter[158], S. Quai[43,37], M. Radovich[57], P.-F. Rocci[50], S. Sacquegna[143,144,145], M. Sahlén[171], D. B. Sanders[66], E. Sarpa[27,28,31], A. Schneider[158], A. Shulevski[172,124,173,174], A. Silvestri[13], L. C. Smith[175], J. Stadel[158], C. Tao[78], G. Testera[17], R. Teyssier[170], S. Tosi[18,128], A. Troja[116,77], M. Tucci[74], C. Valieri[38], A. Venhola[176], D. Vergani[37], F. Vernizzi[177], G. Verza[178], P. Vielzeuf[78], and N. A. Walton[175]

(Affiliations can be found after the references)

May 7, 2026

ABSTRACT

The *Euclid* satellite will provide data on the clustering of galaxies and on the distortion of their measured shapes, which can be used to constrain and test the cosmological model. However, the increase in precision places strong requirements on the accuracy of the theoretical modelling for the observables and of the full analysis pipeline. In this paper, we investigate the accuracy of the calculations performed by the Cosmology Likelihood for Observables in Euclid (`CLOE`), software able to handle both the modelling of observables and their fit against observational data for both the photometric and spectroscopic surveys of *Euclid*, by comparing the output of `CLOE` with external codes used as benchmarks. We perform such a comparison on the quantities entering the calculations of the observables, as well as on the final outputs of these calculations. Our results highlight the high accuracy of `CLOE` when comparing its calculation against external codes for *Euclid* observables on an extended range of operative cases. In particular, all the summary statistics of interest always differ less than $0.1\,\sigma$ from the chosen benchmark, and `CLOE` predictions are statistically compatible with simulated data obtained from benchmark codes. The same holds for the comparison of the correlation function in configuration space for spectroscopic and photometric observables.

Key words. galaxy clustering–weak lensing–*Euclid* survey

1. Introduction

The current decade will see cosmological investigations profit from a significant increase in the precision of data, particularly those related to observations of the large-scale structure (LSS). Several galaxy surveys, such as *Euclid* (Laureijs et al. 2011; Euclid Collaboration: Mellier et al. 2025), the Vera C. Rubin Legacy Survey of Space and Time (LSST; Ivezić et al. 2019), and the *Nancy Grace Roman* Space Telescope (Spergel et al. 2015), will observe the position and shape of billions of galaxies. This will allow us to obtain information on their clustering as well as on the lensing effect that intervening matter has on their shapes, thus effectively mapping the distribution of galaxies and matter across the Universe.

The main goal of such observations is to shed light on the key open questions in the cosmological community, such as understanding the mechanism responsible for the late-time acceleration of the expansion of the Universe (Riess et al. 1998; Perlmutter et al. 1999). Current models range from those that require the presence of a scalar field induced by a dark energy component (Peebles & Ratra 2003) to others that instead invoke a modification of the laws of general relativity on cosmological scales (Clifton et al. 2012). At the same time, other fundamental questions and goals are related to the nature of dark matter (Feng 2010), the measurement of the mass of neutrinos via their impact on the LSS (Lesgourgues & Pastor 2006), as well as the potential detection of primordial non-Gaussianities in the epoch immediately after inflation (Desjacques & Seljak 2010). All of these components leave distinctive imprints on the LSS observables, since they can strongly affect the large-scale matter and galaxy distribution expected from the standard model of cosmology, based on cold pressureless dark matter (CDM) and on a cosmological constant, Λ, the ΛCDM model.

The *Euclid* mission (Laureijs et al. 2011) was specifically designed to tackle these open questions and is expected to deliver a significant improvement in our knowledge in these fields (Euclid Collaboration: Mellier et al. 2025). However, in order to achieve these goals, the exquisite precision of the measurements that will be collected by Stage-IV surveys demands a corresponding level of accuracy in the theoretical modelling of the LSS observables.

For this reason, the Euclid Collaboration has decided to dedicate a major effort to the development of software to compute theoretical predictions for the main scientific observables: the Cosmology Likelihood for Observables in Euclid (`CLOE`). This code implements the modelling of the primary photometric and spectroscopic observables that will be used by *Euclid*, following the theoretical recipe described in Euclid Collaboration: Cardone et al. (2025), hereafter Paper 1. Building a standalone likelihood and theory code for *Euclid* is essential, as we aim to establish a homogeneous and flexible framework that consistently models the primary probes of the mission – weak lensing and galaxy clustering – within a unified approach. Furthermore, the decision to build a new code for the analysis of *Euclid* data allows us to improve the modelling and analysis of systematic effects. Indeed, `CLOE` includes nuisance parameters that capture effects that could be neglected in previous analyses, given the lower sensitivity with respect to *Euclid*. Moreover, it is fully written in `Python`, while still achieving the performance required by a likelihood analysis. More information on these new implementations is provided in Paper 1 and Euclid Collaboration: Joudaki et al. (2026), hereafter Paper 2.

At the practical level, `CLOE` obtains theoretical predictions given a set of cosmological parameters using an interface with `Cobaya`[1] (Torrado & Lewis 2021), which can retrieve the main ingredients for our theoretical expectations from publicly avail-

⋆ e-mail: `matteo.martinelli@inaf.it`

[1] `https://cobaya.readthedocs.io/en/latest/`

able Boltzmann solvers, CAMB[2] (Lewis et al. 2000; Howlett et al. 2012) and CLASS[3] (Blas et al. 2011). The structure of CLOE, its interface with Cobaya, and the way theoretical calculations are performed are presented in detail in Paper 2.

In addition to computation of cosmological observables, the interface with Cobaya allows the user to employ CLOE as a likelihood code, which means comparing theoretical predictions with observational data. By sampling the parameter space and performing this comparison iteratively, CLOE allows us to infer the probability distribution of the free parameters of the model under analysis. This procedure is described in Euclid Collaboration: Cañas-Herrera et al. (2025), hereafter Paper 3, where CLOE is used to derive forecasts on the parameters of the ΛCDM model and some of its extensions (e.g. w_0w_aCDM, non-flat cosmologies) from synthetic *Euclid* data using a realistic set of Markov chain Monte Carlo (MCMC) runs.

The increased precision of the observations that we expect from *Euclid* requires the inclusion of several systematic effects in the modelling of the observables, as neglecting these can produce significant biases in the final results obtained while analysing the data (Tutusaus et al. 2020; Martinelli et al. 2021). Given the complexity of some of the calculations required, it is crucial to assess the accuracy of CLOE, to ensure the quality of the computed theoretical predictions. The choices made in performing the calculations, such as the numerical integrations or the sampling of cosmological functions in redshift and scale, can significantly affect the output of the code and, consequently, the results of the analysis. For this reason, in this paper we aim to compare the calculations performed by CLOE against independent benchmarks, assessing the reliability of this software. This effort is similar to the benchmarking approach taken by other collaborations for codes with similar purposes, such as the Core Cosmology Library (CCL[4], Chisari et al. 2019) developed for LSST (LSST Science Collaboration: Abell et al. 2009; The LSST Dark Energy Science Collaboration: Mandelbaum et al. 2018). Although in this paper our aim is to validate the accuracy of our calculations, the impact of the systematic effects modelled within CLOE will be investigated in a subsequent publication (Euclid Collaboration: Blot et al. 2025).

To reach our goal, we assess the accuracy of the theoretical calculations performed by CLOE, benchmarking them against the results of external codes. We quantify the agreement in units of the observational error, thus ensuring that any difference found is much lower than the statistical uncertainty and, therefore, that it will not impact the real-data analysis. While in this work we provide an assessment of the accuracy of CLOE calculations, an extensive investigation of the methodology used to obtain the observables, their uncertainty, together with a comparison between different non-linear recipes, will be presented in Euclid Collaboration: Crocce et al. (in prep.), Euclid Collaboration: Carrilho et al. (in prep.), Euclid Collaboration: Moretti et al. (in prep.), and Euclid Collaboration: Sciotti et al. (in prep.).

This paper is structured as follows. In Sect. 2 we describe the external codes used to obtain the benchmarks on the observables of interest, while in Sect. 3 we provide details on the settings used for the validation, describing the different effects taken into account, as well as the cosmological assumptions. In Sect. 4, we outline the methods used to validate CLOE against independent codes, and we define the metrics used to assess their agreement. Section 5 contains the validation results for the power spectra observables related to the spectroscopic and photometric observables surveys, including the intermediate quantities that are used to perform these calculations, while Section 6 validates the computation of real-space correlation functions. We draw our conclusions in Sect. 7.

[2] https://camb.readthedocs.io/en/latest/
[3] http://class-code.net/
[4] https://github.com/LSSTDESC/CCL/

Table 1. Summary of connections between equations in Paper 1 and CLOE quantities discussed in this work.

Quantity	Expression	Equation
Weak lensing power spectrum	$C_{ij}^{\rm LL}(\ell)$	(32)
Photometric galaxy power spectrum	$C_{ij}^{\rm GG}(\ell)$	(40)
Galaxy-galaxy lensing power spectrum	$C_{ij}^{\rm GL}(\ell)$	(54)
Weak lensing correlation function	$\xi_{ij}^{\pm}(\theta)$	(70)
Photometric galaxy correlation function	$\xi_{ij}^{\rm GG}(\theta)$	(73)
Galaxy-galaxy lensing correlation function	$\xi_{ij}^{\rm GL}(\theta)$	(74)
Power spectrum Legendre multipoles	$P_\ell(k,z)$	(90)
AP-distorted power spectrum Legendre multipoles	$P_{{\rm obs},\ell}(k^{\rm fid},z)$	(94)
Correlation function Legendre multipoles	$\xi_{{\rm obs},\ell}(s^{\rm fid},z)$	(104)

2. External codes and setup for benchmark generation

As the purpose of this paper is to validate the predictions obtained with CLOE, we compare its results with those of external codes that have previously been validated, at least in a subset of the relevant cases. This section provides a description of these external codes, along with their corresponding references, and outlines the setup adopted to generate the benchmark predictions used for comparison throughout the paper.

In this work, we do not define all the observables that are compared with external codes. The definition of these can be found in Paper 1, where the intermediate quantities used for the calculations are also defined. We report in Table 1 the reference for the equations of the observables that we discuss to facilitate their retrieval in Paper 1.

2.1. External benchmark for 3×2pt

The main observable of the photometric survey of *Euclid* is the set of angular power spectra $C_{ij}^{AB}(\ell)$, defined in Paper 1, for weak lensing (WL), galaxy clustering, and their cross-correlation. These spectra are obtained from CLOE for all the redshift bin combinations given a binned galaxy distribution. We compute $C_{ij}^{AB}(\ell)$ in 270 multipole bins, logarithmically spaced. Similarly, we consider the projection of power spectra in the two points correlation functions (2PCF) $\xi_{ij}^{\rm GG}(\theta)$, $\xi_{ij}^{-}(\theta)$, $\xi_{ij}^{+}(\theta)$, and $\xi_{ij}^{\rm GL}(\theta)$, also defined in Paper 1. These correlation functions are computed in 40 logarithmically spaced bins in the angle θ, contained in the interval $\theta \in [0.1, 10]$ deg.

For what concerns the predictions of CLOE for photometric observables, we rely on two different codes to produce benchmarks: LiFE and CCL. While CCL is a code that has already been extensively used by the cosmological community, this is not the case for LiFE, which is a private code developed to obtain predictions for the *Euclid* survey.

However, due to differences in the assumed recipe, we cannot compare CLOE with CCL for all the cases detailed in Sect. 3. Therefore, we choose to present most of our validation results focusing on LiFE, while we show the outcome of the comparison with CCL, for the cases where this is possible, in Appendix C.

2.1.1. LiFE

LiFE (Likelihood and Forecasts for Euclid) is a collection of codes written in Mathematica[5] to perform the computation of the 3×2pt observables for likelihood evaluation and Fisher matrix forecasts. It has been validated against the code implementation adopted during the Fisher forecast analysis from Euclid Collaboration: Blanchard et al. (2020), checking that, for the same settings, it provides the same estimates of the marginalised constraints on the cosmological parameters, also comparing the intermediate quantities used in calculations. Although not optimised and much slower than any Python implementation, LiFE has been designed with the validation of CLOE in mind. As a consequence, the same exact recipe is also implemented with the possibility of turning on and off different contributions to compare against other codes. For the same reason, it does not compute the matter power spectrum internally, but imports it as an external quantity (to be interpolated) so that one can be sure that any difference with CLOE is not due to errors in this critical quantity. However, the fact that it is coded in a completely different language (with its own interpolation and integration routines) represents a further benefit, allowing us to verify that, for the same input and the same recipe, two independent implementations yield compatible quantities, which is what we want to verify in this work.

LiFE can also be used to perform Fisher matrix forecasts for *Euclid* using the same assumptions (in terms of cosmological model) and settings (e.g. redshift distributions, number of redshift bins, and angular multipoles), adopting a semi-analytic method to compute the derivatives of the observables. Although it is well known that the Fisher matrix method provides lower limits on the marginalised constraints on the cosmological parameters under the assumption of Gaussian likelihood, these forecasts can be used to check that the results from inference are in the same ballpark (see Paper 3).

2.1.2. CCL

CCL is a modern cosmological library designed to compute a large number of cosmological observables for a variety of cosmological models. These range from background quantities, power spectra, and correlation functions to halo model ingredients; it is interfaced with both CAMB – the default choice – and CLASS, and it has been extensively validated against existing codes (Chisari et al. 2019). The core of CCL is developed in C, allowing it to achieve high performance. However, a thoroughly documented Python interface, PyCCL,[6] is also available, combining efficiency and user-friendliness in this way.

For the present exercise, we used the third release of the code (more specifically, v3.0.2). The theory predictions are computed using as input the cosmological parameters, redshift distributions, and systematics defined in Sect. 3.1, as well as the matter power spectrum extracted from CLOE; the growth factor is instead obtained from CCL itself. The harmonic-space power spectra are computed in the Limber approximation via the QAG adaptive integration method of GSL (GNU Scientific Library,[7] Galassi et al. 2009); these are then transformed into the 2PCF via the FFTlog method.

The CCL routines can produce all the cases listed in Table 2, except for the ones including redshift space distortions (RSD) (i.e. P23 and from P11 to P22), for which the implemented recipe differs from the one used in CLOE, which, as outlined in Paper 1, follows Tanidis & Camera (2019). For these cases, only the comparison with LiFE will be shown. The results of the comparison with CCL can be found in Appendix C.

2.2. External benchmark for spectroscopic galaxy clustering (GCsp)

The main observable of the spectroscopic survey of *Euclid* is the set of Legendre multipoles of the anisotropic galaxy power spectrum, $P_{\mathrm{obs},\ell}(k^{\mathrm{fid}}, z)$, as defined in Paper 1 and Euclid Collaboration: Moretti et al. (in prep.). These multipoles are obtained by projecting the two-dimensional anisotropic power spectrum onto the Legendre polynomials $\mathcal{L}_\ell(\mu)$. Under the assumptions of linear theory, only the first three even multipoles are non-vanishing, corresponding to $\ell \in \{0, 2, 4\}$.[8] Similarly, in configuration space, we consider an equivalent expansion over the Legendre polynomials, leading to the 2PCF Legendre multipoles, $\xi_{\mathrm{obs},\ell}(s^{\mathrm{fid}}, z)$.

For the purpose of the validation carried out here, we generate external benchmark predictions without including geometrical distortions caused by adopting a fiducial cosmology that differs from the true one. In other words, we neglect the Alcock–Paczynski (AP; Alcock & Paczynski 1979) effect, which would rescale the transverse, $k_\perp$, and line-of-sight, $k_\parallel$, components of the wavevector k. As a result, the effective quantities we compare are the Legendre multipoles of the power spectrum $P_\ell(k, z)$, computed without AP corrections. Since AP effects depend solely on background quantities, which are validated separately in Appendix D, we do not explore their impact further in this work.

In all cases defined in Sect. 3.2 for the power spectrum Legendre multipoles, the data vectors and covariance matrices are computed at the mean redshift of four distinct redshift bins, namely $\{(0.9, 1.1), (1.1, 1.3), (1.3, 1.5), (1.5, 1.8)\}$, and are sampled using 350 linear k bins in the range $(0.001, 0.35)\,\mathrm{Mpc}^{-1}$. In contrast, for validation carried out in the configuration space, the 2PCF is sampled with linear bins of $\Delta s = 5\,\mathrm{Mpc}$ over the range $(37.5, 387.5)\,\mathrm{Mpc}$.

The external benchmarks are produced using two different codes, PBJ and COFFE. While the former adopts the same non-linear modelling recipe as CLOE in Fourier space, the latter offers a convenient framework to test the pipeline that converts Legendre multipoles from Fourier to configuration space. In the following sections, we briefly summarise the main features of the two codes.

2.2.1. PBJ

The implementation of the non-linear model in CLOE is validated against that in the Power spectrum Bispectrum Joint code (PBJ),[9] a non-public Python package that has been employed in several analyses involving the full shape of the galaxy power spectrum, $P_{\mathrm{gg}}(k)$, and bispectrum, $B_{\mathrm{ggg}}(\boldsymbol{k}_1, \boldsymbol{k}_2)$. These include both comparisons to numerical simulations in the context of model selection (Oddo et al. 2020, 2021), as well as cosmological inference from real data, such as the recent analysis of

[5] Courtesy of V. F. Cardone.
[6] https://ccl.readthedocs.io/en/latest/index.html
[7] http://www.gnu.org/software/gsl/

[8] Non-linear corrections can source non-zero even multipoles with order beyond $\ell = 4$. However, due to their large statistical uncertainties, these additional terms are completely sub-dominant in terms of constraining power and do not carry significant information with respect to the combination $\ell \in \{0, 2, 4\}$.
[9] Courtesy of C. Moretti, E. Sefusatti, A. Oddo.

the BOSS DR12 sample (Euclid Collaboration: Moretti et al. in prep.).

The code features an implementation of the widely adopted effective field theory of large-scale structure (EFTofLSS) model, based on the same theoretical prescription presented in Euclid Collaboration: Pezzotta et al. (2024), which is precisely what has been reproduced in the current version of CLOE. A common feature of models based on non-linear perturbation theory and the EFTofLSS framework is that non-linear corrections to the galaxy (and matter) power spectrum arise from the coupling of different physical scales. This coupling is mediated by kernel functions that encapsulate the physics of gravitational instability, galaxy bias, and RSD. Specifically, the non-linear correction ΔP at a given wavenumber k can be expressed as a convolution of the power spectrum with itself,

$$\Delta P(k) = \int \frac{\mathrm{d}^3 q}{(2\pi)^3} K(\boldsymbol{q}, \boldsymbol{k}-\boldsymbol{q})\, P(\boldsymbol{q})\, P(|\boldsymbol{k}-\boldsymbol{q}|)\,, \tag{1}$$

where the kernel $K(\boldsymbol{q}_1, \boldsymbol{q}_2)$ captures the non-linear mode coupling between the wavemodes $\boldsymbol{q}_1$ and $\boldsymbol{q}_2$. To efficiently evaluate these integrals, PBJ relies on the FASTPT library (McEwen et al. 2016), which takes advantage of the possibility of expanding $K(\boldsymbol{q}_1, \boldsymbol{q}_2)$ in spherical harmonics, enabling the use of fast Fourier transform techniques for rapid and accurate computation.

The implementation of spectroscopic observables in CLOE follows the same approach as PBJ, and both codes adopt identical parametrisation for the EFTofLSS nuisance parameters. This consistency allows for a direct one-to-one comparison of each validation case described in Sect. 3.2, without the need to translate between parameter bases. As a result, we can robustly validate the CLOE predictions for the galaxy power spectrum multipoles $P_\ell(k)$ across all 20 benchmark scenarios presented in Sect. 3.2.

2.2.2. COFFE

Validation of the Legendre multipoles is performed using predictions from the COrrelation Function Full-sky Estimator (COFFE) code[10], a public package designed to efficiently compute two-point statistics in configuration space under linear theory assumptions. In addition to the standard RSD signal, COFFE offers a rigorous treatment of several relativistic effects, including wide-angle corrections and magnification bias. We refer the reader to the COFFE-related literature for further details: theoretical modelling of relativistic effects in the 2PCF is presented in Tansella et al. (2018a), their implementation in Tansella et al. (2018b), and an assessment of the flat-sky approximation in Jelic-Cizmek (2021).

In this work, we employ COFFE to validate the accuracy of the Fourier-to-configuration space mapping used in CLOE, which is based on the numerical evaluation of a Hankel transform. For this purpose, we consider a single benchmark case based on a ΛCDM cosmology with linear-theory predictions, incorporating linear bias and the leading-order RSD effect describing large-scale infall due to galaxy peculiar velocities (Kaiser 1987).

3. Validation settings

One of the main purposes of this validation is to assess the reliability of CLOE when different effects are included in the modelling of *Euclid* observables. For this reason, we compare the predictions of CLOE against other benchmark codes, exploring several combinations of the options available in CLOE. Although we do not perform a full exploration of the parameter space, as would be possible with a Monte Carlo approach, the selected cases are sufficient to validate the main features and systematic effects included in CLOE.

All results presented in this paper were obtained using version v2.0.2 of CLOE,[11] the same version used to derive forecasts in Paper 3. The theoretical framework and implementation details of this version are described in Paper 1 and Paper 2, respectively.

3.1. Photometric settings

For the validation of the photometric observables, we report 23 cases in Table 2 (labelled P01, P02, ..., P23) for which we run our validation pipeline. Switching between these cases, we vary some of the settings available in CLOE to compute the observables. In particular, we focus on variations related to the following quantities.

(i) Cosmology: we choose ten different cosmologies, described in Table 3, where we report the current values ($z = 0$) of the energy density parameters for matter Ω_m, dark energy Ω_DE, and baryons Ω_b, together with the reduced Hubble parameter h, the tilt of the primordial power spectrum n_s, and the perturbation amplitude parameter σ_8. We include ΛCDM extensions such as evolving dark energy equation of state – described by the w_0 and w_a parameters – and non-flat cosmologies – describing scenarios with $\Omega_\mathrm{m} + \Omega_\mathrm{DE} \neq 1$.

(ii) Galaxy distribution $n(z)$: we choose different galaxy redshift distributions, matching the one used in Euclid Collaboration: Blanchard et al. (2020), labelled Inter Science working group Taskforce Forecast (ISTF), the one described in Sect. 5.1 of Paper 1, labelled Science Performance Verification 3 (SPV3), and an intermediate one (Science Performance Verification 2, SPV2), which still contains 13 bins as in SPV3, but with more irregular bin distributions. These choices allow us to test the stability of the code moving from smooth, simple $n(z)$ (ISTF) to more complicated and realistic distributions, investigating potential numerical issues.

(iii) Intrinsic alignment (IA): we choose four cases for this systematic effect, regulated by the three IA parameters $(A_\mathrm{IA}, \eta_\mathrm{IA}, \beta_\mathrm{IA})$. These are cNLA $(0.37, 0.00, 0.00)$, zNLA $(0.16, 1.66, 0.00)$, eNLA $(1.720, -0.41, 2.17)$, and a simple noIA case $(0, 0, 0)$ in which IA is completely neglected (see Paper 1, and references therein). Choosing these different settings allows us to test CLOE in simple scenarios where this systematic effect is absent, as well as different degrees of complexity, by generalising their modelling.

(iv) Galaxy bias $b_\mathrm{g}(z)$: we consider both a binned approach, with one parameter per redshift bin, and a third-order polynomial expression to describe the $b_\mathrm{g}(z)$ function. For the former case, we consider an 'unbiased' case, with all parameters vanishing, a 'linint' case, where $b_\mathrm{g}(z)$ is obtained as the linear interpolation of the binned parameters, and a 'constant' case, where the bias is assumed to be constant in each redshift bin. The two modelling methods tested with these choices provide a stress-test for the reliability of CLOE comparing its performances when switching from a smooth polynomial function to the more agnostic binned approach.

[10] https://github.com/JCGoran/coffe

[11] The theoretical predictions were also benchmarked for v2.1, finding compatible results.

Table 2. Validation cases in which the CLOE calculation of *Euclid* photometric observables are compared with external software.

Id	Cosmology	$n(z)$	IA	galaxy bias	magnification bias	RSD
P01	F1	ISTF	noIA	linint	unbiased	no
P02	F1	ISTF	cNLA	linint	unbiased	no
P03	F1	ISTF	zNLA	linint	unbiased	no
P04	F1	ISTF	eNLA	linint	unbiased	no
P05	F1	ISTF	eNLA	unbiased	unbiased	no
P06	F1	ISTF	eNLA	constant	unbiased	no
P07	F1	SPV2	eNLA	constant	unbiased	no
P08	F1	SPV3	eNLA	constant	unbiased	no
P09	F1	SPV3	eNLA	constant	linint	no
P10	F1	SPV3	eNLA	constant	constant	no
P11	F1	SPV3	eNLA	constant	unbiased	yes
P12	F1	SPV3	eNLA	constant	linint	yes
P13	F1	SPV3	eNLA	constant	constant	yes
P14	F2	SPV3	eNLA	constant	constant	yes
P15	F3	SPV3	eNLA	constant	constant	yes
P16	F4	SPV3	eNLA	constant	constant	yes
P17	F5	SPV3	eNLA	constant	constant	yes
P18	F6	SPV3	eNLA	constant	constant	yes
P19	F7	SPV3	eNLA	constant	constant	yes
P20	F8	SPV3	eNLA	constant	constant	yes
P21	F9	SPV3	eNLA	constant	constant	yes
P22	F10	SPV3	eNLA	constant	constant	yes
P23	F1	SPV3	zNLA	polynomial	polynomial	yes

Table 3. Values of the cosmological parameters in ten cosmologies considered for the validation of cosmological quantities and the main photometric and spectroscopic observables.

Id	$\Omega_{\rm m}$	$\Omega_{\rm DE}$	$\Omega_{\rm b}$	w_0	w_a	h	$n_{\rm s}$	σ_8
F1	0.320	0.680	0.050	−1.000	0.000	0.6737	0.9660	0.8155
F2	0.317	0.676	0.051	−1.017	0.010	0.6775	0.9653	0.8222
F3	0.327	0.670	0.048	−0.913	−0.420	0.6704	0.9561	0.8095
F4	0.316	0.689	0.046	−1.066	0.313	0.6616	0.9524	0.8199
F5	0.321	0.724	0.051	−0.914	−0.050	0.6729	0.9643	0.7996
F6	0.306	0.702	0.047	−1.039	0.046	0.6730	0.9699	0.8248
F7	0.326	0.721	0.050	−0.985	0.428	0.6554	0.9461	0.8059
F8	0.307	0.664	0.045	−1.116	0.268	0.6724	0.9708	0.8273
F9	0.337	0.660	0.053	−0.873	−0.399	0.6658	0.9383	0.8099
F10	0.334	0.630	0.057	−0.903	−0.587	0.6720	0.9779	0.8057

(v) Magnification bias: as for the galaxy bias, we test our calculation modelling the magnification bias using the same approaches as for $b_{\rm g}(z)$.

(vi) RSD: we compare CLOE calculations with the external benchmark in the two available settings for the large-scale RSD effect, that is, when this is considered and when it is neglected. This allows us to test the correct implementation of the RSD model, described in Euclid Collaboration: Tanidis et al. (2024).

Further details on the modelling of the nuisance parameters can be found in Paper 1, while their impact on the cosmological constraints will be discussed in Euclid Collaboration: Blot et al. (2025) also through a more thorough exploration of their parameter space.

Of the cases listed in Table 2, our reference case is P23, which is also based on the settings used to generate synthetic data to obtain forecast results (Paper 3). Although for all cases, we show the summary validation values for all quantities (see Sect. 4), we will highlight in Appendix A more details for our reference, also showing the trends of the differences for each of the validated quantities.

3.2. Spectroscopic settings

In terms of the spectroscopic probe, we identified 20 different cases for the validation, labelled as S01, S02, ..., S20. The first ten cases assume a fixed cosmology (F1 in Table 3) and vary the nuisance parameters,[12] whereas the last ten cases keep the latter fixed and explore the ten different cosmologies shown in Table 3. In terms of nuisance parameters of EFTofLSS, we assume a minimal configuration corresponding to that adopted to obtain MCMC forecasts in Paper 3. This includes six non-zero nuisance parameters, corresponding to the linear b_1 and quadratic bias b_2, three EFTofLSS counterterms (c_0, c_2, c_4) mostly meant to describe the small-scale RSD damping induced by the Fingers of God, and a shot-noise parameter α_P that models constant offsets from Poisson predictions, that is, $1/\overline{n}$ (Ivanov et al. 2020, Euclid Collaboration: Crocce et al. in prep., Euclid Collaboration: Moretti et al. in prep.).

On the other hand, the validation of 2PCF is carried out assuming a single configuration based on linear theory, as described in Sect. 2.2.2. In this case, we assume a ΛCDM cosmology for the comparison. Specifically, the fiducial parameters are $\Omega_{\rm m} = 0.319$, $\Omega_{\rm DE} = 0.681$, $\Omega_{\rm b} = 0.049$, $h = 0.67$, $n_{\rm s} = 0.96$, and $\sigma_8 = 0.83$.

4. Validation methods

The main purpose of this paper is to validate the theoretical predictions for *Euclid* observables obtained by CLOE against external benchmarks. While we are mostly interested in validating the final results, we also examine the intermediate quantities, which are the building blocks of the observables calculation. In this section, we present the different methods used to estimate the agreement between the quantities predicted by CLOE and the corresponding ones from the codes we use as a benchmark. Similarly to what is done for other public codes, such as CCL (see Chisari et al. 2019), we employ different metrics depending on whether or not the quantity under examination is actually observable.

4.1. Symmetric mean absolute percentage error

When assessing the accuracy in our calculations for quantities that are not observables, thus lacking an observational error, we estimate their agreement with the benchmark using the symmetric mean absolute percentage error (SMAPE)

$$\mathrm{SMAPE} = \frac{100}{N}\sum_{i=1}^{N}\frac{\left|F_i^{\rm CLOE} - F_i^{\rm Bench}\right|}{\left(\left|F_i^{\rm CLOE}\right| + \left|F_i^{\rm Bench}\right|\right)/2}\,, \tag{2}$$

where $F_i^{\rm CLOE}$ are the quantities computed by CLOE, $F_i^{\rm Bench}$ is the corresponding benchmark quantity, and the index i runs over the N available elements of the (vectorised) arrays.

The SMAPE estimator has the advantage of quantifying the agreement between two functions relative to the average between the compared quantities, thus without assuming which of the two is correct. Moreover, the SMAPE also allows us to obtain a single value for each of the cases in which we perform our validation (see Sect. 3), thus returning a unique estimation of agreement for each case.

The disadvantage of using this approach is that it does not allow us to observe trends in relation to redshift or scale differences. To address this issue, we also computed the value of the SMAPE at each point in the data vectors and plotted it as a function of redshift or scale, depending on the quantity of interest.

[12] The selected values of the nuisance parameters have been randomly drawn from the marginalised posterior distribution obtained from a specific configuration of the chains run in Paper 3.

4.2. Comparison of observable quantities

While we rely on the SMAPE to assess the difference against benchmark calculations for most quantities, this is not the case for the final observables. For these, we can estimate the observational uncertainty with which *Euclid* can obtain measurements. We choose to estimate our accuracy in terms of this uncertainty.

We define a notion of distance for a given observable O as

$$d_i = \frac{\left|O_i^{\texttt{CLOE}} - O_i^{\texttt{Bench}}\right|}{\sigma_{O_i}}\,, \tag{3}$$

where the index i runs over all the available elements of the observable array, and σ_{O_i} is the observational error associated with each element, obtained using $O_i^{\texttt{Bench}}$ as a reference to compute the error.

The distance defined in Eq. (3) allows us to visualise the difference trend by computing it for each element of the observable array. However, we also want to obtain a single value to quantify the agreement with the benchmark for each validation case. Therefore, we also compute an average and a maximum distance over each observable array, defined as

$$d_{\rm mean} = \frac{1}{N}\sum_{i=1}^{N} d_i\,, \tag{4}$$

$$d_{\rm max} = \max_i d_i\,. \tag{5}$$

With these definitions, it is possible to quantify the agreement between the observables computed by CLOE and the benchmark in terms of the *Euclid* precision. This allows us to define an accuracy threshold above which a difference between our calculation and the benchmark would be too significant to neglect. We set such a threshold to be $d_{\rm max} < 0.1$, defining all quantities for which the distance is within 10% of the observational uncertainty as validated (Massey et al. 2012; Martinelli et al. 2021).

Although the distance defined in Eq. (3) provides an intuitive quantification of the agreement between CLOE and the benchmark codes, and is widely used in the literature (Chisari et al. 2019; Leonard et al. 2023), it has two main drawbacks:

- it does not provide an overall estimate of the statistical compatibility between the prediction of CLOE and those of the benchmark;
- it does not take into account the full observational covariance, since it assumes no correlation between different data bins.

Therefore, we include an additional quantification of the agreement between the codes in terms of χ^2, which allows us to solve these issues.

In order to assess whether the observables computed by CLOE are in agreement with the benchmark within *Euclid* specifications, we compute the reduced χ^2, that is, the χ^2 divided by the number of degrees of freedom $N_{\rm dof}$, obtained by comparing CLOE predictions to those of the benchmark as

$$\chi^2 = (\boldsymbol{B} - \boldsymbol{T})^{\rm T}\ \mathsf{K}^{-1}\ (\boldsymbol{B} - \boldsymbol{T})\,, \tag{6}$$

where $\boldsymbol{B}$ and $\boldsymbol{T}$ are the theory vectors obtained, respectively, from the benchmark and CLOE, while K is the covariance matrix constructed following *Euclid* DR3 specifications and using the benchmark as the fiducial theory predictions.

We impose as a requirement for our comparison that

$$\chi^2 < 0.01\, N_{\rm dof}\,, \tag{7}$$

which corresponds to requiring the difference between the two codes to be within 10% of the observational error.

Photometric survey. Denoting the benchmark spectra as $B_{ij}^{AB}(\ell)$, we compute the observational noise expected for *Euclid* DR3 as (Paper 3)

$$N_{ij}^{\rm GG}(\ell) = \frac{1}{\bar{n}_i}\delta_{ij}^{\rm K}\,, \tag{8}$$

$$N_{ij}^{\rm LL}(\ell) = \frac{\sigma_\epsilon^2}{2\,\bar{n}_i}\delta_{ij}^{\rm K}\,, \tag{9}$$

where $\bar{n}_i$ is the number of observed sources in the i-th redshift bin and σ_ϵ is the intrinsic ellipticity dispersion.

Following the approach of Euclid Collaboration: Sciotti et al. (2024), we use $B_{ij}^{AB}(\ell)$ and $N_{ij}^{AB}(\ell)$ to compute the covariance matrix for each of the cases under examination. The diagonal of the covariance is used to obtain the errors σ_{O_i} used in Eq. (3).

In this work, we use only a Gaussian covariance, neglecting the super-sample and connected non-Gaussian terms, as well as the mode coupling introduced by the mask. For such a reason, we effectively neglect the correlations between different multipoles, obtaining N_ℓ matrices $\mathsf{C}(\ell)$, independent of each other.

For each multipole, we construct a data vector $D_{ij}^{AB}(\ell)$ extracting a random sample from a multivariate normal with mean $B_{ij}^{AB}(\ell)$ and covariance $\mathsf{C}(\ell)$. With this simulated dataset in hand, we can assess the compatibility of the theoretical predictions obtained with CLOE, denoted as $T_{ij}^{AB}(\ell)$, by computing χ^2. This procedure is repeated, generating $N_R = 100$ different realisations of the data vector $D_{ij}^{AB}(\ell)$, and we compute the mean value of χ^2. We then assess whether the prediction of CLOE is compatible with the benchmark spectra by comparing the reduced χ^2 with the limiting values corresponding to the chosen probability threshold.

Spectroscopic survey. Similarly to the previous case, the covariance matrix for the galaxy power spectrum multipoles is derived only considering the Gaussian limit, as described in Grieb et al. (2016). In this way, the bin-averaged covariance can be written as

$$C_{\ell_1\ell_2}(k_i, k_j) = \frac{2\,(2\pi^4)}{V_{k_i}^2}\,\delta_{ij}^{\rm K}\int_{k_i-\Delta k/2}^{k_i+\Delta k/2}\sigma_{\ell_1\ell_2}^2(k)\,k^2\,{\rm d}\,k\,, \tag{10}$$

where the per-mode covariance is defined as

$$\sigma_{\ell_1\ell_2}^2(k) = \frac{(2\,\ell_1+1)\,(2\,\ell_2+1)}{V_{\rm s}} \times \int_{-1}^{+1}\left[P_{\rm gg}(k,\mu) + \frac{1}{\bar{n}}\right]^2 \mathcal{L}_{\ell_1}(\mu)\,\mathcal{L}_{\ell_2}(\mu)\,{\rm d}\mu\,, \tag{11}$$

as in the corresponding equations of Paper 1 (see Table 1). Here, μ is the cosine of the angle between the wavemode $\boldsymbol{k}$ and the line of sight, $\bar{n}$ is the mean number density of the individual spectroscopic bins, $V_{k_i} = 4\,\pi\,[(k_i + \Delta k/2)^3 - (k_i - \Delta k/2)^3]/3$ is the volume of the spherical shell centred at k_i with width Δk, and $V_{\rm s}$ is the volume of the considered redshift bin. In this limit, the cross-covariance terms are zero by construction, except for the covariance of different multipoles $P_\ell(k)$ at the same wavenumber k.

For the purpose of validation, we consider a volume for each spectroscopic bin corresponding to the one already introduced in Sect. 2.2, with centres at $z \in \{1, 1.2, 1.4, 1.65\}$ and $\Delta z \in \{0.2, 0.2, 0.2, 0.3\}$. The chosen number density corresponds to

the one predicted from a luminosity function of Hα galaxies corresponding to Model 3 in Pozzetti et al. (2016), which was already adopted in other preparation analyses of *Euclid* (e.g. Euclid Collaboration: Pezzotta et al. 2024). In this case, we also use the diagonal of the covariance to obtain the errors σ_{O_i} used in Eq. (3).

A more complete theoretical covariance, also accounting for the impact of the super-survey modes and the trispectrum contribution (Wadekar & Scoccimarro 2020) within the geometry defined by the *Euclid* angular footprint, will be considered for the analysis of DR1 data. The technical implementation of such covariance will be described in dedicated papers (Euclid Collaboration: Salvalaggio et al. in prep., Euclid Collaboration: Sciotti et al. in prep.). The calculation of the χ^2 statistics is then consistent with that of Eq. (6), with the corresponding change of theory and data vectors and covariance matrices.

5. Validation results

In this section, we validate the cosmological quantities computed by CLOE, as well as the observables for the photometric and spectroscopic surveys across the different configuration cases described in Sect. 3, following the methodology outlined in Sect. 4. For clarity, we divide the validation into separate subsections, focusing individually on cosmological background quantities, photometric observables, and spectroscopic observables.

5.1. Cosmological functions

Before we focus our attention on the observables computed by CLOE and their agreement with the external benchmarks, we first want to scrutinise the agreement in the cosmological functions that are the building blocks for such quantities, namely the comoving distance $r(z)$, the normalised Hubble parameter $E(z) = H(z)/H_0$, with H_0 the Hubble constant, that is, the present-time value of the Hubble parameter, the growth factor $g_+(z)$, and the two transverse comoving distances $f_K(z)$ and $f_K(z_1, z_2)$, accounting for possible spatial curvature. As shown in Sect. 2 of Paper 1, these quantities enter all the predictions made by CLOE, and therefore any difference would propagate to the final observables.

CLOE extracts $E(z)$ and $r(z)$ directly from a Boltzmann solver (either CAMB or CLASS), while it computes the other quantities internally. Given that both CAMB and CLASS have been extensively validated, we can safely assume that the quantities that we retrieve from these codes do not present any issue. However, it is necessary to assess the reliability of the cosmological quantities computed by CLOE, namely $g_+(z)$ and the comoving distances $f_K(z)$ and $f_K(z_1, z_2)$. We present this comparison in Fig. 1, where we show, for all cosmologies considered, the SMAPE of the cosmological quantities internally computed by CLOE with respect to those which can be retrieved from CAMB.[13]

We notice that the distance functions $f_K(z)$ and $f_K(z_1, z_2)$ agree very well with those computed by CAMB, with the SMAPE always staying several orders of magnitude below the 1% level. Furthermore, the change in cosmological parameters does not lead to any significant difference in the comparison, as can be seen by the overlap of the lines corresponding to different cosmologies in Fig. 1. However, we observe larger differences in the growth factor $g_+(z)$. This is because while CAMB obtains this

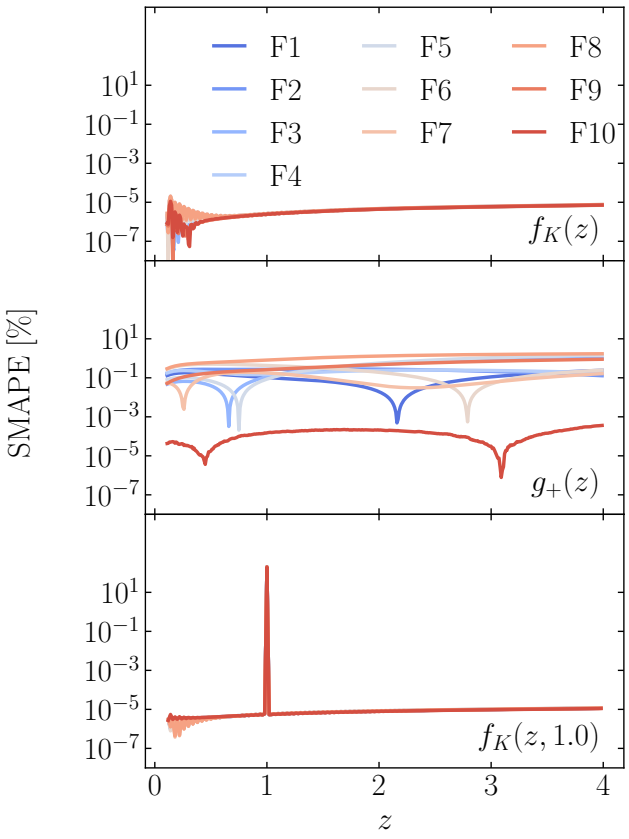

Fig. 1. Comparison of the cosmological quantities internally computed by CLOE with those extracted from CAMB for the cosmologies listed in Table 3. Please note that CAMB automatically sets $f_K(z_1, z_2) = 0$ when $z_1 > z_2$, while CLOE returns its absolute value for any redshift combination. In order to perform this comparison, we symmetrise the results obtained from CAMB. The spikes visible in the comparison of the $f_K(z_1, z_2)$ values are due to this function vanishing when $z_1 = z_2$. We only show the transverse distance $f_K(z_1, z_2)$ with $z_2 = 1$, with the other cases showing the same behaviour.

quantity by solving the differential equation for matter perturbation δ_m, CLOE computes $g_+(z)$ by taking the ratio of the matter power spectra at different redshifts and at a reference scale (see Eq. 22 of Paper 1, for details on this calculations). Despite these differences, the comparison still yields results within 1% accuracy. However, a revised version of CLOE will aim to further improve this comparison by extracting this quantity directly from the Boltzmann solvers through Cobaya.

It is important to stress that throughout this validation we use CLOE interfaced with CAMB. As discussed in Paper 2, CLOE can also be interfaced with CLASS. However, at the time our comparison was performed, our baseline recipe for non-linear corrections, HMCode2020 (Mead et al. 2021), was not available in CLASS, making it impossible to apply the full validation pipeline by interfacing CLOE with CLASS. Nevertheless, in Appendix D we show a comparison between the main cosmological quantities used in the calculation of theoretical predictions between CLOE + CLASS and CLOE + CAMB.

5.2. Photometric 3×2pt observables

In this section, we apply the validation metrics discussed in Sect. 4 to the photometric observables, namely the $C_{ij}^{AB}(\ell)$ power spectra for all tracers and redshift bin combinations (see Sect. 3 of

[13] We refer the reader to Torrado & Lewis (2021) for a comparison between CAMB and the quantities which can be extracted by interfacing Cobaya with Boltzmann solvers.

Paper 1). We refer the reader to Appendix B for a discussion of the intermediate quantities entering the calculation of the $C_{ij}^{AB}(\ell)$.

In Fig. 2, we show in the left panel the mean and maximum distances for each of the validation cases, while in the right panel we report the value of the reduced χ^2 (solid lines), obtained by dividing the results of Eq. (6) by the number of degrees of freedom $N_{\rm dof}$ corresponding to each case. We show the trend of such a quantity for the two photometric observables (WL and photometric galaxy clustering, GCph), their cross-correlation (galaxy-galaxy lensing, GGL) and, for the χ^2 calculation, their combination (3×2pt). We find that, in all validation cases, both the distance in units of the expected error and the reduced χ^2 fall within the threshold values, highlighting the statistical compatibility of the theoretical predictions of CLOE with those of the benchmark code. Furthermore, we can see how the two tests yield very similar results, highlighting how the χ^2 test reaches, despite accounting for the off-diagonal terms of the covariance, the same performance as the distance test, where such terms are neglected.

We notice how all observables exhibit better agreement for the P01–P06 cases. This is because these cases assume the galaxy distribution of ISTF, which is a distribution that is split into fewer bins and whose functions are much smoother than in other validation cases. This allows us to reduce numerical and interpolation errors with respect to other galaxy distributions when computing the kernel functions, thus yielding a better comparison. We refer the reader to Appendix B for a visualisation of kernel validation in the different cases. Overall, we find no significant discrepancy between the benchmark and the predictions of CLOE, independently of the observable analysed or of the validation case.

5.3. Spectroscopic galaxy clustering observable

In this section, we validate the implementation of the model relevant for the spectroscopic probe of *Euclid*. The validation of intermediate quantities, such as the individual contributions entering the perturbative expansion of the reference non-linear model implemented in CLOE, will be presented in a dedicated paper (Euclid Collaboration: Crocce et al. in prep.). Here, we restrict our analysis to the final spectroscopic observables, namely the Legendre multipoles $P_\ell(k, z)$ of the anisotropic galaxy power spectrum.

The main results of the validation are presented in Fig. 3. Here we show the distance metrics between CLOE and PBJ as defined in Eqs. (4) and (5), considering all redshift bins, multipole orders, and validation cases. Since the recipe for the anisotropic galaxy power spectrum $P_{\rm gg}(k, \mu)$ in CLOE follows the same implementation as in PBJ, we find a good match between the two sets of predictions, with a relative error that always stays below 10% of the statistical error. This happens not only when considering the mean distance between the two sets of predictions but also with the maximum distance. Given this level of agreement, the average reduced χ^2 values obtained by comparing the theory vectors generated by CLOE and PBJ are also extremely good, as we show in Fig. 4. Quantitatively, the average χ^2 is entirely within the 68% confidence region of the corresponding χ^2 distribution with the same number of degrees of freedom. Residual fluctuations are primarily due to differences in the unit conventions adopted by the two codes (i.e. choosing Mpc^{-1} against $h\,\mathrm{Mpc}^{-1}$), which can induce small discrepancies in the computation of the internal components of the loop expansion, as well as in the algorithms used to project the 2D power spectrum onto the Legendre polynomials. While this section focuses only on the distance metrics and averaged χ^2 statistics, a direct comparison of the theory vectors for a reference case is presented in Appendix A.2.

6. Comparison of real-space correlation functions

In Sect. 5.2 and 5.3, we assessed the validity of CLOE focusing on the harmonic-space power spectra $C_{ij}^{AB}(\ell)$ and the Legendre multipole $P_{{\rm obs},\ell}(k^{\rm fid}, z)$ as the observables to be compared. However, several analyses of LSS data in the literature rely instead on two-point correlation functions in real space. For the photometric survey, these are the galaxy correlation function $\xi_{ij}^{\rm GG}$, the two lensing correlations ξ_{ij}^{+} and ξ_{ij}^{-}, and the galaxy-galaxy lensing correlation $\xi_{ij}^{\rm GL}$, while for the spectroscopic survey, we are interested in the 2PCF Legendre multipoles $\xi_{{\rm obs},\ell}(s^{\rm fid}, z)$.

In the comparison performed in Sect. 5, we relied on the intuitive definition of distance defined in Eq. (3), obtaining the error σ_{O_i} from the diagonal of the covariance matrices. However, this requires that the off-diagonal terms in the covariances are negligible, which is not the case for 2PCF (see e.g. Eisenstein & Zaldarriaga 2001). This can be easily observed in Figs. 5 and 6, where we show the correlation matrix for the photometric and spectroscopic cases.

This implies that the error obtained by taking the diagonal of these matrices would yield a significant underestimation of the uncertainties with respect to what would be obtained by considering the full covariances. For such a reason, in comparing the photometric and spectroscopic 2PCF we rely only on the χ^2 estimate of Eq. (6), avoiding the computation of the distance in units of error.

Furthermore, CLOE computes the 2PCF by projecting the observables validated in Sect. 5. For such a reason, we do not repeat the validation for all the cases discussed in Sect. 3, deeming it sufficient to perform the validation in the reference cases, P23 and S01 for the photometric and spectroscopic surveys, respectively.

For the photometric correlation functions, we perform the validation by computing the covariance matrix using the public OneCovariance code (Reischke et al. 2025).[14] This computes the covariance in harmonic space and then projects it into real space using the equations presented in Joachimi et al. (2021).

For the spectroscopic correlation functions, similar to the case in Fourier space, we only make use of the Gaussian limit, which translates to a conservative validation of the implementation in CLOE. In this case, the covariance matrices for the four different spectroscopic bins have been computed using the public GaussianCovariance code.[15]

We present the results of our comparison in Table 4, where it is possible to notice how the reduced χ^2 value obtained for 2PCF is within the expected limits for both photometric and spectroscopic surveys, with the exception of $\xi_{ij}^{\rm GG}$, for which the difference between CLOE and the benchmark is within 20% of the observational error, rather than the required 10%. While such a discrepancy will not affect constraints in a significant way, in future developments we will assess the possible numerical differences that yield such a result.

[14] https://github.com/rreischke/OneCovariance
[15] https://gitlab.com/veropalumbo.alfonso/gaussiancovariance

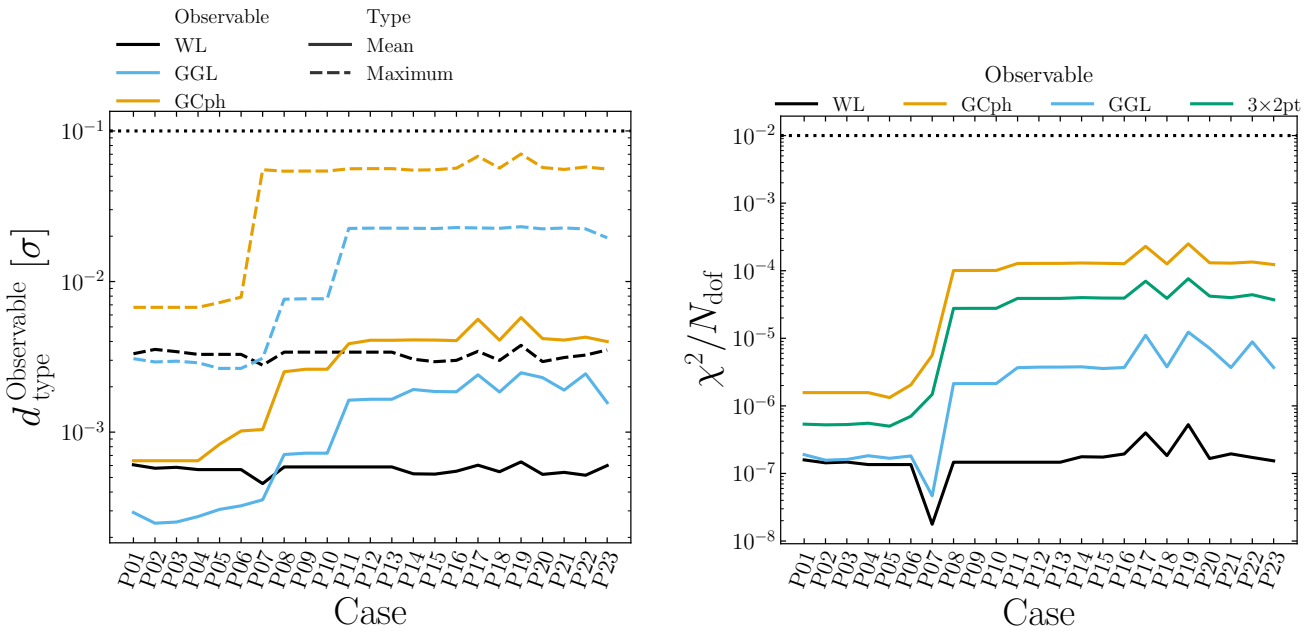

Fig. 2. *Left panel:* Distance in units of the expected error for the three photometric observables, both when averaged over the multipoles (solid lines) and taking the highest value of the distance (dashed lines). The dotted black line indicates our threshold of $d = 0.1\,\sigma$. *Right panel:* Solid lines show the reduced χ^2 value for WL (black), GCph (orange), GGL (cyan), and their combination (green). The dashed line represents the limiting value of the reduced χ^2 that we choose to be 0.01. The results are shown for the different cases described in Table 2.

Table 4. Reduced χ^2 for 2PCF of photometric (top row) and spectroscopic (bottom row) observables.

	Photometric			
	ξ^{GG}_{ij}	ξ^{GL}_{ij}	ξ^{-}_{ij}	ξ^{+}_{ij}
χ^2/N_{dof}	0.040	0.001	6×10^{-5}	5×10^{-5}
	Spectroscopic			
	$z = 1.0$	$z = 1.2$	$z = 1.4$	$z = 1.65$
χ^2/N_{dof}	7×10^{-4}	5×10^{-4}	4×10^{-4}	4×10^{-4}

7. Conclusions

The main objective of this work was to benchmark the code used to obtain theoretical predictions for *Euclid* observables: `CLOE`. In order to do so, we compared these predictions with those obtained from external software that implements the same recipe.

Although we do not explore the parameter space systematically, we performed this benchmarking in a wide set of validation cases, described in Sect. 3. This allowed us to test the features implemented in `CLOE`, which are described in detail in Paper 1.

After presenting the methodology to quantify the discrepancy between `CLOE` and the benchmark in Sect. 4, and the external codes used as benchmarks in Sect. 2, we compared as a first step the basic cosmological ingredients of our recipe in Sect. 5.1. Here we found a sub-percent agreement between `CLOE` and `LiFE` for all functions in all the chosen cosmologies and, even more importantly, we found a very good agreement between `CLOE` and `CAMB`. For the latter comparison, we found that the most significant difference is obtained for the growth factor $g_+(z)$; the internal calculation of `CLOE` approximates this with the square root of a ratio of matter power spectra, which, when compared with the `CAMB` prediction, yields a discrepancy of 1 percent. Following the validation of these fundamental ingredients, we focused separately on the two surveys of *Euclid*: spectroscopic and photometric.

In Sect. 5.3, we discussed the validation of the final spectroscopic observables against an external code, `PBJ`, which implements the same model for the spectroscopic galaxy power spectrum based on the EFTofLSS framework. For this comparison, we only considered the final *Euclid* observables, the power spectrum Legendre multipoles, while we left the benchmarking of intermediate quantities to a dedicated work (Euclid Collaboration: Crocce et al. in prep., Euclid Collaboration: Moretti et al. in prep.). We computed a distance metric between the two codes based on a *Euclid*-like statistical uncertainty that assumes only the Gaussian limit, therefore providing a much more conservative comparison than if also including non-Gaussian contributions. We found an optimal agreement between `CLOE` and `PBJ`, with a distance metric that stays consistently below the 10 percent expected statistical error for all redshifts and wavemodes. Furthermore, the χ^2 analysis shows that the theoretical predictions of `CLOE` are in statistical agreement with the dataset generated using `PBJ`.

The validation of the photometric observables was presented in Sect. 5.2, where we obtained the results of the distance and χ^2 tests for the calculation of $C^{AB}_{ij}(\ell)$, comparing the calculations of `CLOE` with those of `LiFE`. We show in Fig. 2 how, in all our validation cases, both the distances and the reduced χ^2 are well within their limiting values for the chosen probability threshold (68%). We find no significant differences for the separate photometric observables or their combination, as well as no significant trend with the analysed cases, except for a better agreement found in the case P01–P06, where we use a smooth galaxy distribution. Thus, we can conclude that the harmonic power spectra of `CLOE` are statistically compatible with the benchmark within the expected DR3 errors of *Euclid*.

In addition to the final observables for this survey, we also validated the implementation of intermediate calculations. We

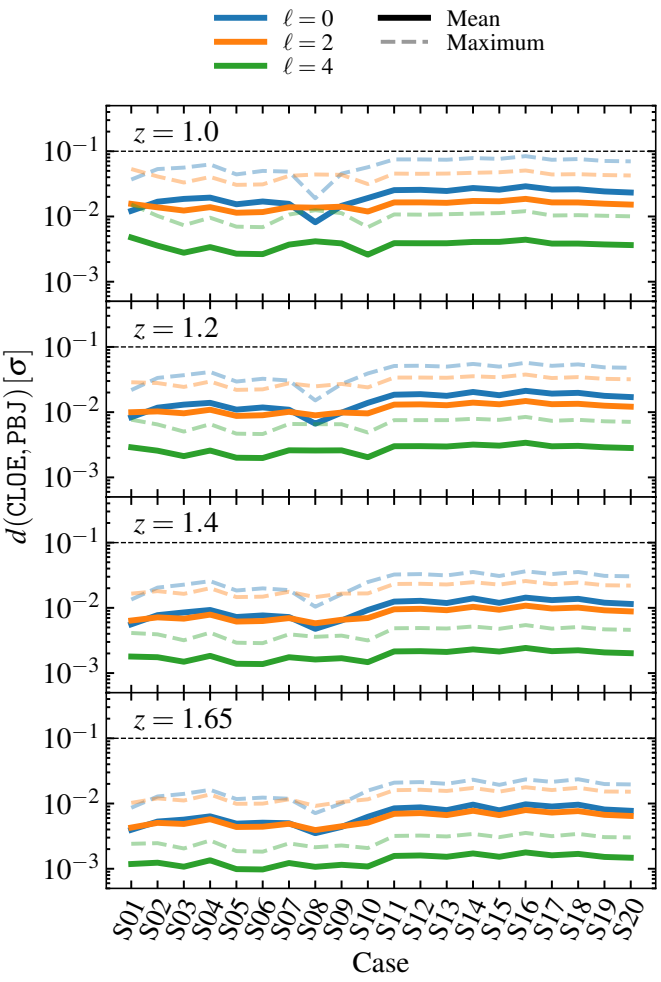

Fig. 3. Maximum relative difference between CLOE and PBJ in units of a Gaussian standard deviation obtained with the configuration described in Sect. 4.2. Different panels correspond to different redshifts, as shown in the corresponding top left corners. Different multipoles are identified by the different colours, while solid and dashed lines mark the average and maximum difference along the sampled k values, respectively. The dotted horizontal line in each panel marks the threshold of 10% of the statistical error.

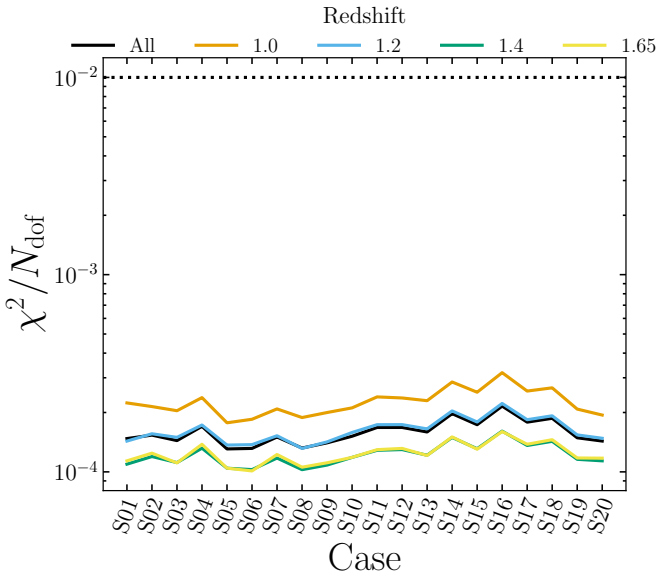

Fig. 4. Reduced χ^2 displayed in the 20 validation cases for the GCsp probe combination. As in Fig. 2, the dotted line shows the limiting threshold of the χ^2, corresponding to the requirement of CLOE departing from the benchmark by less than 10% of the observational error.

presented in Appendix B the validation of the kernel functions $W_i^A(z)$, the power spectra for galaxies, matter, and intrinsic alignment. We found these functions to be compatible with the benchmark well within 1 percent, with the worst performance found for the power spectra containing the intrinsic alignment terms, which are those related to the growth factor $g_+(z)$.

In Section A, we showed a more detailed comparison for a single case. For the photometric observables, we chose the P23 case as a reference, showing in Fig. A.1 the distance in units of the observational errors as a function of the multipole ℓ, for each observable. Similarly, in Fig. A.2 we showed the trends in k of the distance for the spectroscopic observables, choosing as a reference the S01 case.

Similarly, the validation of the 2PCF Legendre multipoles points towards an optimal consistency of the implementation present in CLOE with the one produced by COFFE. In this case, given the non-negligible contributions of the off-diagonal terms in the covariance, we only performed the χ^2 analysis, reported in Table 4, finding good statistical agreement between the CLOE predictions and the benchmark.

In Table 4, we also report the results of the χ^2 analysis for photometric 2PCFs, obtained as a projection of $C_{ij}^{AB}(\ell)$. In this case, we also find good agreement with the benchmark: all observables are well within our chosen threshold, with the exception of $\xi_{ij}^{\rm GG}$ whose difference with respect to LiFE is within 20% of the statistical error, rather than the required 10%. Given that our requirements are quite stringent, we are confident that such a difference will not propagate to biases on parameter estimation. However, our future goal is to investigate the source of this difference to reduce it to the required threshold.

Thanks to the results obtained in this paper, we conclude that CLOE is reliable and accurate software, able to compute *Euclid*'s main observables efficiently while in agreement with other software. We are therefore confident that the final results obtained with *Euclid* will have negligible bias resulting from the theoretical calculations we examined in this work.

Acknowledgements. The Euclid Consortium acknowledges the European Space Agency and a number of agencies and institutes that have supported the development of *Euclid*, in particular the Agenzia Spaziale Italiana, the Austrian Forschungsförderungsgesellschaft funded through BMK, the Belgian Science Policy, the Canadian Euclid Consortium, the Deutsches Zentrum für Luft- und Raumfahrt, the DTU Space and the Niels Bohr Institute in Denmark, the French Centre National d'Etudes Spatiales, the Fundação para a Ciência e a Tecnologia, the Hungarian Academy of Sciences, the Ministerio de Ciencia, Innovación y Universidades, the National Aeronautics and Space Administration, the National Astronomical Observatory of Japan, the Netherlandse Onderzoekschool Voor Astronomie, the Norwegian Space Agency, the Research Council of Finland, the Romanian Space Agency, the State Secretariat for Education, Research, and Innovation (SERI) at the Swiss Space Office (SSO), and the United Kingdom Space Agency. A complete and detailed list is available on the *Euclid* web site (www.euclid-ec.org). MM acknowledges funding by the Agenzia Spaziale Italiana (ASI) under agreement no. 2018-23-HH.0 and support from INFN/Euclid Sezione di Roma. SC acknowledges support from the Italian Ministry of University and Research (MUR), PRIN 2022 'EXSKALIBUR – Euclid-Cross-SKA: Likelihood Inference Building for Universe's Research', Grant No. 20222BBYB9, CUP D53D2300252 0006, and from the European Union – Next Generation EU. SD acknowledges support from the Italian Ministry of University and Research (MUR), PRIN 2022 'LaScaLa - Large Scale Lab', Grant No. 20222JBEKN, founded by the European Union – Next Generation EU. During part of this work, AMCLB was supported by a Paris Observatory-PSL University Fellowship, hosted at the Paris Observatory. SP acknowledges support through

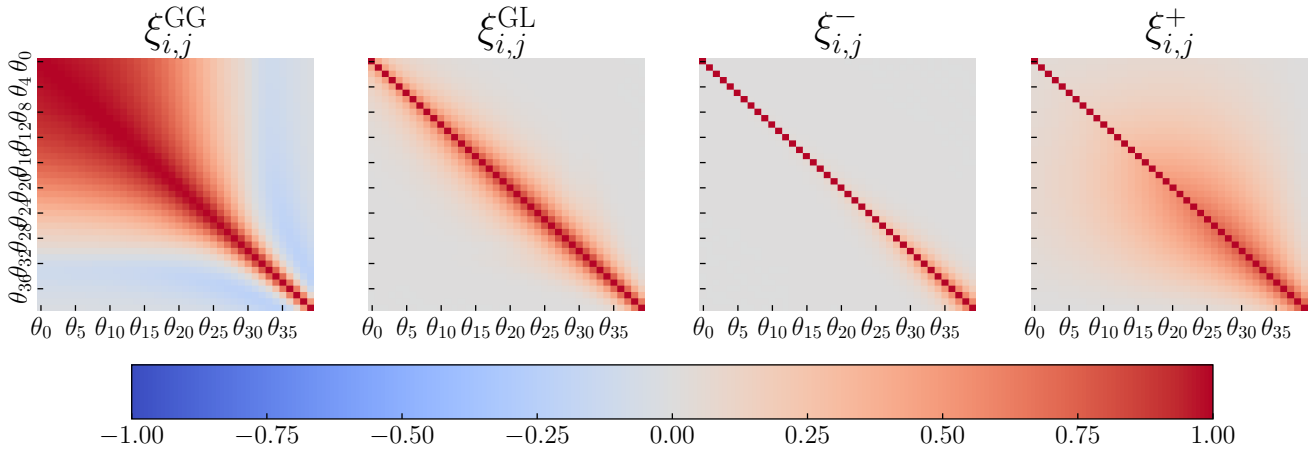

Fig. 5. Correlation matrices between the different angles θ_i for which the 2PCF are computed, taken for $i = j = 6$ in the P23 case.

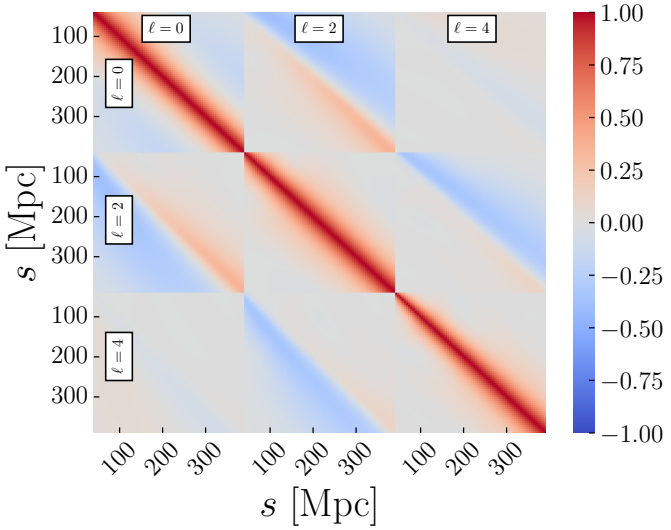

Fig. 6. Correlation matrix of the linear-theory 2PCF multipoles assuming the setup adopted for the validation, thus linear bias and RSD signal, and number density corresponding to the ones defined in Paper 3.

the *Conception Arenal Programme* of the Universidad de Cantabria and funding from the project UC-LIME (PID2022-140670NA-I00), financed by MCIN AEI/10.13039/501100011033/FEDER, UE. The authors acknowledge the contribution of the Lorentz Center (Leiden), and of the European Space Agency (ESA), where the workshop "Making CLOE shine" and the "CLOE workshop 2023" were held.

References

Alcock, C. & Paczynski, B. 1979, Nature, 281, 358
Blas, D., Lesgourgues, J., & Tram, T. 2011, JCAP, 07, 034
Chisari, N. E., Alonso, D., Krause, E., et al. 2019, ApJS, 242, 2
Clifton, T., Ferreira, P. G., Padilla, A., & Skordis, C. 2012, Physics Reports, 513, 1
Desjacques, V. & Seljak, U. 2010, Clas. Quan. Grav., 27, 124011
Eisenstein, D. J. & Zaldarriaga, M. 2001, ApJ, 546, 2
Euclid Collaboration: Blanchard, A., Camera, S., Carbone, C., et al. 2020, A&A, 642, A191
Euclid Collaboration: Blot, L., Tanidis, K., Cañas-Herrera, G., et al. 2025, A&A, submitted, arXiv:2510.10021
Euclid Collaboration: Cañas-Herrera, G., Goh, L. W. K., Blot, L., et al. 2025, A&A, submitted, arXiv:2510.09153
Euclid Collaboration: Cardone, V. F., Joudaki, S., Blot, L., et al. 2025, A&A, accepted, arXiv:2510.09118
Euclid Collaboration: Joudaki, S. et al. 2026, A&A, accepted, arXiv:2510.09118
Euclid Collaboration: Mellier, Y., Abdurro'uf, Acevedo Barroso, J., et al. 2025, A&A, 697, A1
Euclid Collaboration: Pezzotta, A., Moretti, C., Zennaro, M., et al. 2024, A&A, 687, A216
Euclid Collaboration: Sciotti, D., Gouyou Beauchamps, S., Cardone, V. F., et al. 2024, A&A, 691, A318
Euclid Collaboration: Tanidis, K., Cardone, V. F., Martinelli, M., et al. 2024, A&A, 683, A17
Feng, J. L. 2010, ARA&A, 48, 495
Galassi, M., Davies, J., Theiler, J., et al. 2009, GNU Scientific Library Reference Manual, 3rd edn. (Network Theory Ltd.)
Grieb, J. N., Sánchez, A. G., Salazar-Albornoz, S., & Dalla Vecchia, C. 2016, MNRAS, 457, 1577
Howlett, C., Lewis, A., Hall, A., & Challinor, A. 2012, JCAP, 04, 027
Ivanov, M. M., Simonović, M., & Zaldarriaga, M. 2020, JCAP, 05, 042
Ivezić, Ž., Kahn, S. M., Tyson, J. A., et al. 2019, ApJ, 873, 111
Jelic-Cizmek, G. 2021, JCAP, 07, 045
Joachimi, B., Lin, C. A., Asgari, M., et al. 2021, A&A, 646, A129
Kaiser, N. 1987, MNRAS, 227, 1
Laureijs, R., Amiaux, J., Arduini, S., et al. 2011, ESA/SRE(2011)12, arXiv:1110.3193
Leonard, C. D. et al. 2023, Open Journal of Astrophysics, 6, 1
Lesgourgues, J. & Pastor, S. 2006, Physics Reports, 429, 307
Lewis, A., Challinor, A., & Lasenby, A. 2000, ApJ, 538, 473
LSST Science Collaboration: Abell, P. A., Allison, J., Anderson, S. F., et al. 2009, arXiv:0912.0201
Martinelli, M., Tutusaus, I., Archidiacono, M., et al. 2021, A&A, 649, A100
Massey, R., Hoekstra, H., Kitching, T., et al. 2012, MNRAS, 429, 661
McEwen, J. E., Fang, X., Hirata, C. M., & Blazek, J. A. 2016, JCAP, 09, 015
Mead, A. J., Brieden, S., Tröster, T., & Heymans, C. 2021, MNRAS, 502, 1401
Oddo, A., Rizzo, F., Sefusatti, E., Porciani, C., & Monaco, P. 2021, JCAP, 11, 038
Oddo, A., Sefusatti, E., Porciani, C., Monaco, P., & Sánchez, A. G. 2020, JCAP, 03, 056
Peebles, P. J. E. & Ratra, B. 2003, Rev. Mod. Phys., 75, 559
Perlmutter, S., Aldering, G., Goldhaber, G., et al. 1999, ApJ, 517, 565
Pozzetti, L., Hirata, C. M., Geach, J. E., et al. 2016, A&A, 590, A3
Reischke, R., Unruh, S., Asgari, M., et al. 2025, A&A, 699, A124
Riess, A. G., Filippenko, A. V., Challis, P., et al. 1998, AJ, 116, 1009
Spergel, D., Gehrels, N., Baltay, C., et al. 2015, arXiv:1503.03757
Tanidis, K. & Camera, S. 2019, MNRAS, 489, 3385
Tansella, V., Bonvin, C., Durrer, R., Ghosh, B., & Sellentin, E. 2018a, JCAP, 03, 019
Tansella, V., Jelic-Cizmek, G., Bonvin, C., & Durrer, R. 2018b, JCAP, 10, 032
The LSST Dark Energy Science Collaboration: Mandelbaum, R., Eifler, T., Hložek, R., et al. 2018, arXiv:1809.01669
Torrado, J. & Lewis, A. 2021, JCAP, 05, 057
Tutusaus, I., Martinelli, M., Cardone, V. F., et al. 2020, A&A, 643, A70
Wadekar, D. & Scoccimarro, R. 2020, Phys. Rev. D, 102, 123517

[1] INAF-Osservatorio Astronomico di Roma, Via Frascati 33, 00078 Monteporzio Catone, Italy
[2] INFN-Sezione di Roma, Piazzale Aldo Moro, 2 - c/o Dipartimento di Fisica, Edificio G. Marconi, 00185 Roma, Italy
[3] INAF-Osservatorio Astronomico di Brera, Via Brera 28, 20122 Milano, Italy
[4] Max Planck Institute for Extraterrestrial Physics, Giessenbachstr. 1, 85748 Garching, Germany
[5] Center for Data-Driven Discovery, Kavli IPMU (WPI), UTIAS, The University of Tokyo, Kashiwa, Chiba 277-8583, Japan
[6] Laboratoire Univers et Théorie, Observatoire de Paris, Université PSL, Université Paris Cité, CNRS, 92190 Meudon, France
[7] INAF-IASF Milano, Via Alfonso Corti 12, 20133 Milano, Italy
[8] Waterloo Centre for Astrophysics, University of Waterloo, Waterloo, Ontario N2L 3G1, Canada
[9] Dipartimento di Fisica, Università degli Studi di Torino, Via P. Giuria 1, 10125 Torino, Italy
[10] INFN-Sezione di Torino, Via P. Giuria 1, 10125 Torino, Italy
[11] INAF-Osservatorio Astrofisico di Torino, Via Osservatorio 20, 10025 Pino Torinese (TO), Italy
[12] European Space Agency/ESTEC, Keplerlaan 1, 2201 AZ Noordwijk, The Netherlands
[13] Institute Lorentz, Leiden University, Niels Bohrweg 2, 2333 CA Leiden, The Netherlands
[14] Leiden Observatory, Leiden University, Einsteinweg 55, 2333 CC Leiden, The Netherlands
[15] Institute for Astronomy, University of Edinburgh, Royal Observatory, Blackford Hill, Edinburgh EH9 3HJ, UK
[16] Institute for Theoretical Particle Physics and Cosmology (TTK), RWTH Aachen University, 52056 Aachen, Germany
[17] INFN-Sezione di Genova, Via Dodecaneso 33, 16146, Genova, Italy
[18] Dipartimento di Fisica, Università di Genova, Via Dodecaneso 33, 16146, Genova, Italy
[19] Université Paris-Saclay, Université Paris Cité, CEA, CNRS, AIM, 91191, Gif-sur-Yvette, France
[20] Institut d'Estudis Espacials de Catalunya (IEEC), Edifici RDIT, Campus UPC, 08860 Castelldefels, Barcelona, Spain
[21] Institute of Space Sciences (ICE, CSIC), Campus UAB, Carrer de Can Magrans, s/n, 08193 Barcelona, Spain
[22] Université Paris-Saclay, CNRS/IN2P3, IJCLab, 91405 Orsay, France
[23] Institut de Recherche en Astrophysique et Planétologie (IRAP), Université de Toulouse, CNRS, UPS, CNES, 14 Av. Edouard Belin, 31400 Toulouse, France
[24] Centro de Investigaciones Energéticas, Medioambientales y Tecnológicas (CIEMAT), Avenida Complutense 40, 28040 Madrid, Spain
[25] Institute of Cosmology and Gravitation, University of Portsmouth, Portsmouth PO1 3FX, UK
[26] Laboratoire d'etude de l'Univers et des phenomenes eXtremes, Observatoire de Paris, Université PSL, Sorbonne Université, CNRS, 92190 Meudon, France
[27] SISSA, International School for Advanced Studies, Via Bonomea 265, 34136 Trieste TS, Italy
[28] ICSC - Centro Nazionale di Ricerca in High Performance Computing, Big Data e Quantum Computing, Via Magnanelli 2, Bologna, Italy
[29] INAF-Osservatorio Astronomico di Trieste, Via G. B. Tiepolo 11, 34143 Trieste, Italy
[30] IFPU, Institute for Fundamental Physics of the Universe, via Beirut 2, 34151 Trieste, Italy
[31] INFN, Sezione di Trieste, Via Valerio 2, 34127 Trieste TS, Italy
[32] Institut für Theoretische Physik, University of Heidelberg, Philosophenweg 16, 69120 Heidelberg, Germany
[33] Université St Joseph; Faculty of Sciences, Beirut, Lebanon
[34] Department of Physics, Oxford University, Keble Road, Oxford OX1 3RH, UK
[35] Institute for Particle Physics and Astrophysics, Dept. of Physics, ETH Zurich, Wolfgang-Pauli-Strasse 27, 8093 Zurich, Switzerland
[36] LINKS Foundation, Via Pier Carlo Boggio, 61 10138 Torino, Italy
[37] INAF-Osservatorio di Astrofisica e Scienza dello Spazio di Bologna, Via Piero Gobetti 93/3, 40129 Bologna, Italy
[38] INFN-Sezione di Bologna, Viale Berti Pichat 6/2, 40127 Bologna, Italy
[39] DAMTP, Centre for Mathematical Sciences, Wilberforce Road, Cambridge CB3 0WA, UK
[40] Kavli Institute for Cosmology Cambridge, Madingley Road, Cambridge, CB3 0HA, UK
[41] Dipartimento di Fisica e Scienze della Terra, Università degli Studi di Ferrara, Via Giuseppe Saragat 1, 44122 Ferrara, Italy
[42] Istituto Nazionale di Fisica Nucleare, Sezione di Ferrara, Via Giuseppe Saragat 1, 44122 Ferrara, Italy
[43] Dipartimento di Fisica e Astronomia "Augusto Righi" - Alma Mater Studiorum Università di Bologna, via Piero Gobetti 93/2, 40129 Bologna, Italy
[44] Université de Genève, Département de Physique Théorique and Centre for Astroparticle Physics, 24 quai Ernest-Ansermet, CH-1211 Genève 4, Switzerland
[45] Instituto de Física de Cantabria, Edificio Juan Jordá, Avenida de los Castros, 39005 Santander, Spain
[46] Higgs Centre for Theoretical Physics, School of Physics and Astronomy, The University of Edinburgh, Edinburgh EH9 3FD, UK
[47] Aix-Marseille Université, Université de Toulon, CNRS, CPT, Marseille, France
[48] Jodrell Bank Centre for Astrophysics, Department of Physics and Astronomy, University of Manchester, Oxford Road, Manchester M13 9PL, UK
[49] Université Libre de Bruxelles (ULB), Service de Physique Théorique CP225, Boulevard du Triophe, 1050 Bruxelles, Belgium
[50] Université Paris-Saclay, CNRS, Institut d'astrophysique spatiale, 91405, Orsay, France
[51] Departamento de Física, FCFM, Universidad de Chile, Blanco Encalada 2008, Santiago, Chile
[52] Mathematical Institute, University of Leiden, Einsteinweg 55, 2333 CA Leiden, The Netherlands
[53] Center for Cosmology and AstroParticle Physics, The Ohio State University, 191 West Woodruff Avenue, Columbus, OH 43210, USA
[54] Department of Physics, The Ohio State University, Columbus, OH 43210, USA
[55] ESAC/ESA, Camino Bajo del Castillo, s/n., Urb. Villafranca del Castillo, 28692 Villanueva de la Cañada, Madrid, Spain
[56] Dipartimento di Fisica e Astronomia, Università di Bologna, Via Gobetti 93/2, 40129 Bologna, Italy
[57] INAF-Osservatorio Astronomico di Padova, Via dell'Osservatorio 5, 35122 Padova, Italy
[58] Universitäts-Sternwarte München, Fakultät für Physik, Ludwig-Maximilians-Universität München, Scheinerstrasse 1, 81679 München, Germany
[59] Space Science Data Center, Italian Space Agency, via del Politecnico snc, 00133 Roma, Italy
[60] Department of Physics "E. Pancini", University Federico II, Via Cinthia 6, 80126, Napoli, Italy
[61] INAF-Osservatorio Astronomico di Capodimonte, Via Moiariello 16, 80131 Napoli, Italy
[62] Instituto de Astrofísica e Ciências do Espaço, Universidade do Porto, CAUP, Rua das Estrelas, PT4150-762 Porto, Portugal
[63] Faculdade de Ciências da Universidade do Porto, Rua do Campo de Alegre, 4150-007 Porto, Portugal
[64] Port d'Informació Científica, Campus UAB, C. Albareda s/n, 08193 Bellaterra (Barcelona), Spain
[65] INFN section of Naples, Via Cinthia 6, 80126, Napoli, Italy
[66] Institute for Astronomy, University of Hawaii, 2680 Woodlawn Drive, Honolulu, HI 96822, USA
[67] Dipartimento di Fisica e Astronomia "Augusto Righi" - Alma Mater Studiorum Università di Bologna, Viale Berti Pichat 6/2, 40127 Bologna, Italy
[68] Instituto de Astrofísica de Canarias, Vía Láctea, 38205 La Laguna,

Tenerife, Spain
[69] European Space Agency/ESRIN, Largo Galileo Galilei 1, 00044 Frascati, Roma, Italy
[70] Université Claude Bernard Lyon 1, CNRS/IN2P3, IP2I Lyon, UMR 5822, Villeurbanne, F-69100, France
[71] UCB Lyon 1, CNRS/IN2P3, IUF, IP2I Lyon, 4 rue Enrico Fermi, 69622 Villeurbanne, France
[72] Departamento de Física, Faculdade de Ciências, Universidade de Lisboa, Edifício C8, Campo Grande, PT1749-016 Lisboa, Portugal
[73] Instituto de Astrofísica e Ciências do Espaço, Faculdade de Ciências, Universidade de Lisboa, Campo Grande, 1749-016 Lisboa, Portugal
[74] Department of Astronomy, University of Geneva, ch. d'Ecogia 16, 1290 Versoix, Switzerland
[75] Aix-Marseille Université, CNRS, CNES, LAM, Marseille, France
[76] INAF-Istituto di Astrofisica e Planetologia Spaziali, via del Fosso del Cavaliere, 100, 00100 Roma, Italy
[77] INFN-Padova, Via Marzolo 8, 35131 Padova, Italy
[78] Aix-Marseille Université, CNRS/IN2P3, CPPM, Marseille, France
[79] INFN-Bologna, Via Irnerio 46, 40126 Bologna, Italy
[80] School of Physics, HH Wills Physics Laboratory, University of Bristol, Tyndall Avenue, Bristol, BS8 1TL, UK
[81] Dipartimento di Fisica "Aldo Pontremoli", Università degli Studi di Milano, Via Celoria 16, 20133 Milano, Italy
[82] INFN-Sezione di Milano, Via Celoria 16, 20133 Milano, Italy
[83] Institute of Theoretical Astrophysics, University of Oslo, P.O. Box 1029 Blindern, 0315 Oslo, Norway
[84] Jet Propulsion Laboratory, California Institute of Technology, 4800 Oak Grove Drive, Pasadena, CA, 91109, USA
[85] Felix Hormuth Engineering, Goethestr. 17, 69181 Leimen, Germany
[86] Technical University of Denmark, Elektrovej 327, 2800 Kgs. Lyngby, Denmark
[87] Cosmic Dawn Center (DAWN), Denmark
[88] Institut d'Astrophysique de Paris, UMR 7095, CNRS, and Sorbonne Université, 98 bis boulevard Arago, 75014 Paris, France
[89] Max-Planck-Institut für Astronomie, Königstuhl 17, 69117 Heidelberg, Germany
[90] NASA Goddard Space Flight Center, Greenbelt, MD 20771, USA
[91] Department of Physics and Astronomy, University College London, Gower Street, London WC1E 6BT, UK
[92] Department of Physics and Helsinki Institute of Physics, Gustaf Hällströmin katu 2, 00014 University of Helsinki, Finland
[93] Department of Physics, P.O. Box 64, 00014 University of Helsinki, Finland
[94] Helsinki Institute of Physics, Gustaf Hällströmin katu 2, University of Helsinki, Helsinki, Finland
[95] Mullard Space Science Laboratory, University College London, Holmbury St Mary, Dorking, Surrey RH5 6NT, UK
[96] SKA Observatory, Jodrell Bank, Lower Withington, Macclesfield, Cheshire SK11 9FT, UK
[97] Centre de Calcul de l'IN2P3/CNRS, 21 avenue Pierre de Coubertin 69627 Villeurbanne Cedex, France
[98] University of Applied Sciences and Arts of Northwestern Switzerland, School of Engineering, 5210 Windisch, Switzerland
[99] Universität Bonn, Argelander-Institut für Astronomie, Auf dem Hügel 71, 53121 Bonn, Germany
[100] Department of Physics, Institute for Computational Cosmology, Durham University, South Road, Durham, DH1 3LE, UK
[101] Université Côte d'Azur, Observatoire de la Côte d'Azur, CNRS, Laboratoire Lagrange, Bd de l'Observatoire, CS 34229, 06304 Nice cedex 4, France
[102] Université Paris Cité, CNRS, Astroparticule et Cosmologie, 75013 Paris, France
[103] CNRS-UCB International Research Laboratory, Centre Pierre Binétruy, IRL2007, CPB-IN2P3, Berkeley, USA
[104] Institut d'Astrophysique de Paris, 98bis Boulevard Arago, 75014, Paris, France
[105] Institute of Physics, Laboratory of Astrophysics, Ecole Polytechnique Fédérale de Lausanne (EPFL), Observatoire de Sauverny, 1290 Versoix, Switzerland
[106] Aurora Technology for European Space Agency (ESA), Camino bajo del Castillo, s/n, Urbanizacion Villafranca del Castillo, Villanueva de la Cañada, 28692 Madrid, Spain
[107] Institut de Física d'Altes Energies (IFAE), The Barcelona Institute of Science and Technology, Campus UAB, 08193 Bellaterra (Barcelona), Spain
[108] School of Mathematics, Statistics and Physics, Newcastle University, Herschel Building, Newcastle-upon-Tyne, NE1 7RU, UK
[109] DARK, Niels Bohr Institute, University of Copenhagen, Jagtvej 155, 2200 Copenhagen, Denmark
[110] Department of Physics and Astronomy, University of Waterloo, Waterloo, Ontario N2L 3G1, Canada
[111] Perimeter Institute for Theoretical Physics, Waterloo, Ontario N2L 2Y5, Canada
[112] Centre National d'Etudes Spatiales – Centre spatial de Toulouse, 18 avenue Edouard Belin, 31401 Toulouse Cedex 9, France
[113] Institute of Space Science, Str. Atomistilor, nr. 409 Măgurele, Ilfov, 077125, Romania
[114] Consejo Superior de Investigaciones Cientificas, Calle Serrano 117, 28006 Madrid, Spain
[115] Universidad de La Laguna, Departamento de Astrofísica, 38206 La Laguna, Tenerife, Spain
[116] Dipartimento di Fisica e Astronomia "G. Galilei", Università di Padova, Via Marzolo 8, 35131 Padova, Italy
[117] Universität Innsbruck, Institut für Astro- und Teilchenphysik, Technikerstr. 25/8, 6020 Innsbruck, Austria
[118] Satlantis, University Science Park, Sede Bld 48940, Leioa-Bilbao, Spain
[119] Department of Physics, Royal Holloway, University of London, TW20 0EX, UK
[120] Instituto de Astrofísica e Ciências do Espaço, Faculdade de Ciências, Universidade de Lisboa, Tapada da Ajuda, 1349-018 Lisboa, Portugal
[121] Cosmic Dawn Center (DAWN)
[122] Niels Bohr Institute, University of Copenhagen, Jagtvej 128, 2200 Copenhagen, Denmark
[123] Universidad Politécnica de Cartagena, Departamento de Electrónica y Tecnología de Computadoras, Plaza del Hospital 1, 30202 Cartagena, Spain
[124] Kapteyn Astronomical Institute, University of Groningen, PO Box 800, 9700 AV Groningen, The Netherlands
[125] Infrared Processing and Analysis Center, California Institute of Technology, Pasadena, CA 91125, USA
[126] INAF, Istituto di Radioastronomia, Via Piero Gobetti 101, 40129 Bologna, Italy
[127] Astronomical Observatory of the Autonomous Region of the Aosta Valley (OAVdA), Loc. Lignan 39, I-11020, Nus (Aosta Valley), Italy
[128] INAF-Osservatorio Astronomico di Brera, Via Brera 28, 20122 Milano, Italy, and INFN-Sezione di Genova, Via Dodecaneso 33, 16146, Genova, Italy
[129] ICL, Junia, Université Catholique de Lille, LITL, 59000 Lille, France
[130] Instituto de Física Teórica UAM-CSIC, Campus de Cantoblanco, 28049 Madrid, Spain
[131] CERCA/ISO, Department of Physics, Case Western Reserve University, 10900 Euclid Avenue, Cleveland, OH 44106, USA
[132] Technical University of Munich, TUM School of Natural Sciences, Physics Department, James-Franck-Str. 1, 85748 Garching, Germany
[133] Max-Planck-Institut für Astrophysik, Karl-Schwarzschild-Str. 1, 85748 Garching, Germany
[134] Donostia International Physics Center (DIPC), Paseo Manuel de Lardizabal, 4, 20018, Donostia-San Sebastián, Guipuzkoa, Spain
[135] IKERBASQUE, Basque Foundation for Science, 48013, Bilbao, Spain
[136] Departamento de Física Fundamental. Universidad de Salamanca. Plaza de la Merced s/n. 37008 Salamanca, Spain
[137] Université de Strasbourg, CNRS, Observatoire astronomique de

Strasbourg, UMR 7550, 67000 Strasbourg, France
[138] Ludwig-Maximilians-University, Schellingstrasse 4, 80799 Munich, Germany
[139] Max-Planck-Institut für Physik, Boltzmannstr. 8, 85748 Garching, Germany
[140] Dipartimento di Fisica - Sezione di Astronomia, Università di Trieste, Via Tiepolo 11, 34131 Trieste, Italy
[141] California Institute of Technology, 1200 E California Blvd, Pasadena, CA 91125, USA
[142] Department of Physics & Astronomy, University of California Irvine, Irvine CA 92697, USA
[143] Department of Mathematics and Physics E. De Giorgi, University of Salento, Via per Arnesano, CP-I93, 73100, Lecce, Italy
[144] INFN, Sezione di Lecce, Via per Arnesano, CP-193, 73100, Lecce, Italy
[145] INAF-Sezione di Lecce, c/o Dipartimento Matematica e Fisica, Via per Arnesano, 73100, Lecce, Italy
[146] Departamento Física Aplicada, Universidad Politécnica de Cartagena, Campus Muralla del Mar, 30202 Cartagena, Murcia, Spain
[147] Observatorio Nacional, Rua General Jose Cristino, 77-Bairro Imperial de Sao Cristovao, Rio de Janeiro, 20921-400, Brazil
[148] CEA Saclay, DFR/IRFU, Service d'Astrophysique, Bat. 709, 91191 Gif-sur-Yvette, France
[149] Department of Computer Science, Aalto University, PO Box 15400, Espoo, FI-00 076, Finland
[150] Instituto de Astrofísica de Canarias, c/ Via Lactea s/n, La Laguna 38200, Spain. Departamento de Astrofísica de la Universidad de La Laguna, Avda. Francisco Sanchez, La Laguna, 38200, Spain
[151] Caltech/IPAC, 1200 E. California Blvd., Pasadena, CA 91125, USA
[152] Ruhr University Bochum, Faculty of Physics and Astronomy, Astronomical Institute (AIRUB), German Centre for Cosmological Lensing (GCCL), 44780 Bochum, Germany
[153] Department of Physics and Astronomy, Vesilinnantie 5, 20014 University of Turku, Finland
[154] Serco for European Space Agency (ESA), Camino bajo del Castillo, s/n, Urbanizacion Villafranca del Castillo, Villanueva de la Cañada, 28692 Madrid, Spain
[155] ARC Centre of Excellence for Dark Matter Particle Physics, Melbourne, Australia
[156] Centre for Astrophysics & Supercomputing, Swinburne University of Technology, Hawthorn, Victoria 3122, Australia
[157] Department of Physics and Astronomy, University of the Western Cape, Bellville, Cape Town, 7535, South Africa
[158] Department of Astrophysics, University of Zurich, Winterthurerstrasse 190, 8057 Zurich, Switzerland
[159] Department of Physics, Centre for Extragalactic Astronomy, Durham University, South Road, Durham, DH1 3LE, UK
[160] IRFU, CEA, Université Paris-Saclay 91191 Gif-sur-Yvette Cedex, France
[161] Oskar Klein Centre for Cosmoparticle Physics, Department of Physics, Stockholm University, Stockholm, SE-106 91, Sweden
[162] Astrophysics Group, Blackett Laboratory, Imperial College London, London SW7 2AZ, UK
[163] Univ. Grenoble Alpes, CNRS, Grenoble INP, LPSC-IN2P3, 53, Avenue des Martyrs, 38000, Grenoble, France
[164] INAF-Osservatorio Astrofisico di Arcetri, Largo E. Fermi 5, 50125, Firenze, Italy
[165] Dipartimento di Fisica, Sapienza Università di Roma, Piazzale Aldo Moro 2, 00185 Roma, Italy
[166] Centro de Astrofísica da Universidade do Porto, Rua das Estrelas, 4150-762 Porto, Portugal
[167] Dipartimento di Fisica, Università di Roma Tor Vergata, Via della Ricerca Scientifica 1, Roma, Italy
[168] INFN, Sezione di Roma 2, Via della Ricerca Scientifica 1, Roma, Italy
[169] HE Space for European Space Agency (ESA), Camino bajo del Castillo, s/n, Urbanizacion Villafranca del Castillo, Villanueva de la Cañada, 28692 Madrid, Spain
[170] Department of Astrophysical Sciences, Peyton Hall, Princeton University, Princeton, NJ 08544, USA
[171] Theoretical astrophysics, Department of Physics and Astronomy, Uppsala University, Box 516, 751 37 Uppsala, Sweden
[172] ASTRON, the Netherlands Institute for Radio Astronomy, Postbus 2, 7990 AA, Dwingeloo, The Netherlands
[173] Anton Pannekoek Institute for Astronomy, University of Amsterdam, Postbus 94249, 1090 GE Amsterdam, The Netherlands
[174] Center for Advanced Interdisciplinary Research, Ss. Cyril and Methodius University in Skopje, Macedonia
[175] Institute of Astronomy, University of Cambridge, Madingley Road, Cambridge CB3 0HA, UK
[176] Space physics and astronomy research unit, University of Oulu, Pentti Kaiteran katu 1, FI-90014 Oulu, Finland
[177] Institut de Physique Théorique, CEA, CNRS, Université Paris-Saclay 91191 Gif-sur-Yvette Cedex, France
[178] Center for Computational Astrophysics, Flatiron Institute, 162 5th Avenue, 10010, New York, NY, USA

Appendix A: Reference case comparison

In Sects. 5.2 and 5.3 we compare the predictions of CLOE with those of the benchmark in a variety of cases, exploring different features that are available in CLOE. Here, instead, we present the comparison in more detail in a specific case, that is, the one used as a fiducial to obtain the results presented in Paper 3.

A.1. Photometric survey

For the photometric survey, we choose as a reference the P23 case, and we show in Fig. A.1 the trends in multipoles of the distance in units of the error for WL, GCph, and their cross-correlation GGL. We find no significant trend with the multipoles ℓ and no significant difference between the analysed probes. We find GCph to be the observable with the highest values of this distance, compatible with the results presented in Sect. 5.2, which is a direct result of the smaller observational error for this observable with respect to the others.

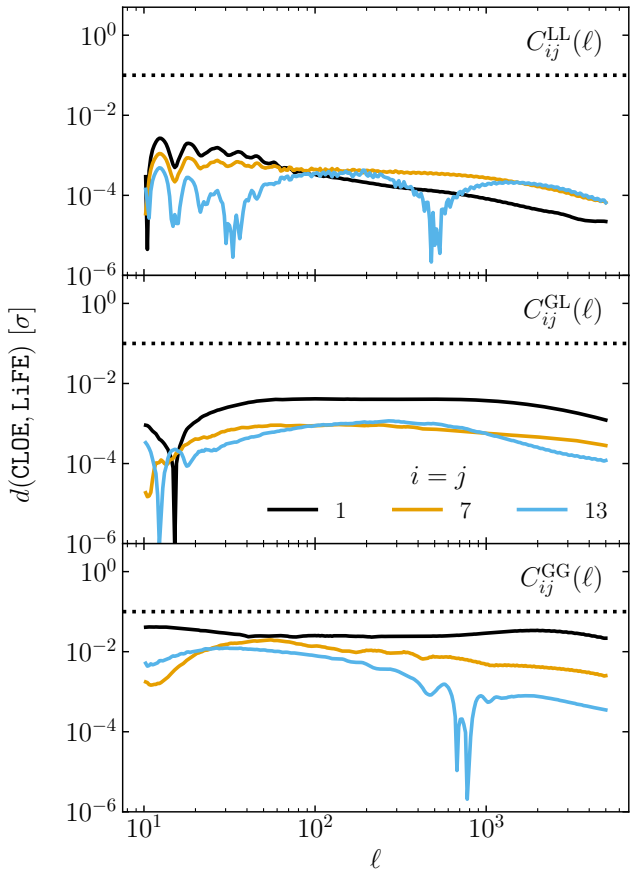

Fig. A.1. Distance in units of the expected error as a function of the multipole ℓ for WL (*top panel*), GCph (*bottom panel*), and their cross-correlation GGL (*middle panel*). The different colours indicate the redshift bin considered. The black dotted line shows the threshold value of $0.1\,\sigma$. This comparison is performed in the reference case P23.

A.2. Spectroscopic survey

In Fig. A.2, we show the distance metric as a function of the wavemode k for a reference case, a flat ΛCDM cosmology as in case S01. In all panels, we show the accuracy between CLOE and PBJ using two sets of predictions: in the first one, each code

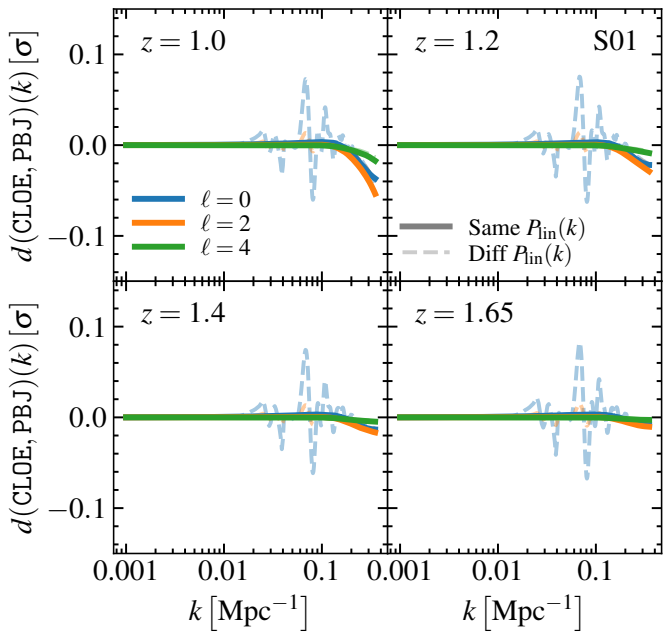

Fig. A.2. Systematic difference between CLOE and PBJ for the case S01 (flat ΛCDM) of GCsp. The difference is quantified in terms of the distance metric defined in Eqs. (5) and (4). Different colours correspond to different multipoles, while solid and dashed lines denote the case when CLOE and PBJ use the same input linear power spectrum or not, respectively.

obtains the linear power spectrum predictions from an individual call to the Boltzmann solver (CAMB in this case), while, in the second one, the same linear predictions are used consistently across the two codes. In the first case, we observe residuals in the final Legendre multipoles that are always smaller than 10% of the corresponding statistical error for a few spurious positions along the k axis, mostly concentrated over the BAO scales. This is a consequence of employing slightly different versions and accuracy flags in the Boltzmann solver, but despite this difference, the trend is to have an optimal consistency in terms of the broadband of the multipoles. The agreement is even better when considering the same input spectra, for which we only observe a minor deviation at $k \gtrsim 0.1\,{\rm Mpc}^{-1}$ that is induced by a small difference in the way infrared resummation is carried out in the two codes. This is mostly due to the different set of units adopted by the two codes, with or without h, respectively (Euclid Collaboration: Moretti et al. in prep.).

Appendix B: Photometric intermediate quantities

In Sect. 5.2, we quantified the departures of CLOE predictions for photometric observables with respect to the chosen benchmark code. Here, instead, we apply our validation methodology to the intermediate quantities related to the photometric survey of *Euclid*, mainly the kernel functions and the power spectra (see Sect. 3 of Paper 1). In this section, we show the validation results across the cases described in Sect. 3, highlighting the overall comparison of these quantities.

The first set of intermediate quantities that we focus on are the kernel functions entering the expression for photometric observables, namely the shear kernel $W_i^{\gamma}(z)$, the magnification kernel $W_i^{\mu}(z)$, the galaxy kernel $W_i^{\rm g}(z)$, and the intrinsic alignment kernel $W_i^{\rm IA}(z)$.

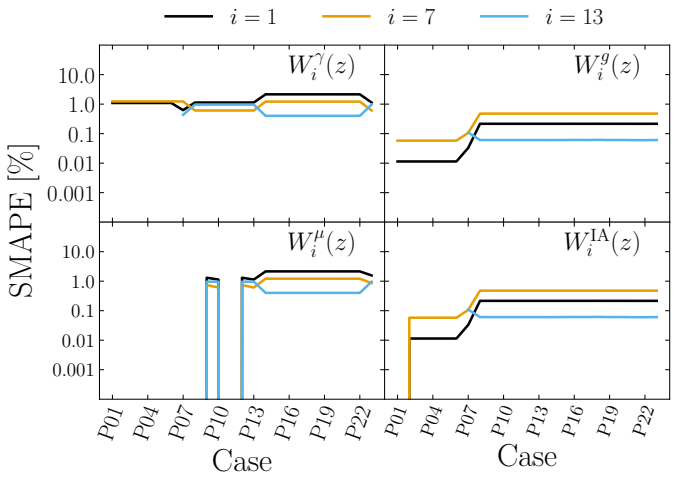

Fig. B.1. Summary SMAPE values for the kernels comparison between CLOE and LiFE in the different cases investigated. Each colour refers to a different redshift bin of the tomographic *Euclid* analysis. The figure shows the comparison result in each case for representative redshift bins at low ($i = 1$, black lines), intermediate ($i = 7$, orange lines) and high redshift ($i = 13$, cyan lines). Notice that for the cases P01 to P06, this latter bin is not available, as the $n(z)$ is divided into only 10 tomographic bins. The specifications of the different cases are reported in Table 2.

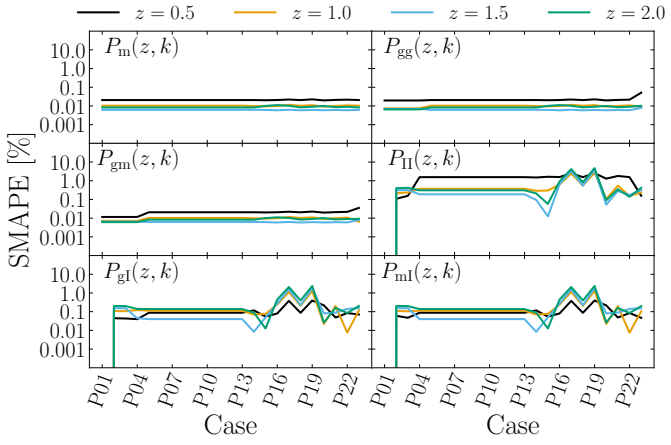

Fig. B.2. Summary comparison for the intermediate power spectra, as computed by CLOE and LiFE. For each of the different power spectra, shown in separate panels, we show the comparison at different redshifts. The specifications of the different cases are reported in Table 2.

We report the overall value of the SMAPE for the four kernels in Fig. B.1. Here we can notice how the SMAPE values are of the order of one per cent, with W_i^γ and W_i^μ being the kernels with the worst agreement. This deviation is caused by the fact that the calculation of these functions requires an integration of the binned galaxy redshift distribution (see Paper 1); if such a distribution is not smooth, differences in the numerical sampling between the codes can propagate to the final kernel computations. Indeed, it can be noticed how the cases P01–P06 yield a generally better comparison, as these cases assume the ISTF galaxy redshift distribution (Euclid Collaboration: Blanchard et al. 2020), which is more regular and with broader bins with respect to the other two, limiting the impact of numerical errors.

Following the validation of the kernel functions, we shift our attention to the power spectra entering the calculation of the photometric observables (see section 3.1 of Paper 1). These are the matter power spectrum $P_{\rm m}(k, z)$, the galaxy power spectrum $P_{\rm gg}(k, z)$, and the intrinsic alignment power spectrum $P_{\rm II}(k, z)$, together with all cross combinations $P_{\rm gm}$, $P_{\rm gI}$, and $P_{\rm mI}$.

We report the overall value of the SMAPE for the six power spectra, computed at four different redshifts, in Fig. B.2. It is possible to notice how the comparison does not exhibit a strong case dependency, with mostly constant trends for the SMAPE values at all redshifts and for all spectra. Nevertheless, it is possible to see a dependency on the chosen case for the P13–P22 cases, where the cosmological parameters change in value, in the power spectra containing the intrinsic alignment contribution. This trend can be connected to the differences between the two codes in the growth factor $g_+(z)$, discussed in Sect. 5.1.

Appendix C: Comparison with CCL

The comparison against CCL has proceeded as described above for LiFE. To compute the final observables of interest (2PCF and power spectra), the code requires as external input the $n(z)$, the tabulated values of galaxy and magnification bias, and the tabulated IA kernel. The $C_{ij}^{AB}(\ell)$ are then computed, using the Limber approximation, using quadrature integration (which is the most accurate and for which the best agreement is found) as mentioned in Sect. 2.1.2. To be as accurate as possible, we boost some of the accuracy settings, such as the number of points in z and k used for the power spectrum splines and the number of points at which the kernels are evaluated.

The results of the comparison, shown in Fig. C.1, are below the $0.1\,\sigma$ threshold for all the cases investigated, which, as mentioned above, are all the cases without RSD.

Generally, the distance between CLOE and CCL increases with the complexity of the source and lens redshift distribution, as is also the case for the comparison against LiFE (see Fig. 2); this is an expected result, and is more prominent for GCph since the relative kernels are much less smooth and have narrower support. The few cases above the threshold are indeed only for the maximum GCph discrepancy, and only concern individual or very small sets of ℓ values. As can be seen in the bottom panel of Fig. 2, such differences do not lead to statistical incompatibilities.

Appendix D: Cosmology with CLOE + CLASS

The results and main conclusions that we draw in this work are obtained using CLOE interfaced to the Boltzmann solver CAMB, through the structure of Cobaya (see Paper 2). However, CLOE has been built having in mind the possibility of switching between CAMB and CLASS without any significant change in the pipeline.

At the time of this comparison, the version of CLASS interfaced does not allow us to use the non-linear recipe we identified as our baseline choice (HMCODE2020), and therefore we cannot apply to the CLOE + CLASS configuration the same validation pipeline we used for CLOE + CAMB.

Nevertheless, the calculations performed by CLOE are independent of the choice made on the Boltzmann solver, on which the code relies only to obtain a set of basic cosmological ingredients, used in the calculations. For such a reason, to assess the agreement between CLOE + CAMB and CLOE + CLASS, it is enough to compare these functions in the two cases, as all subsequent calculations will be identical, whatever the choice for the Boltzmann solver is.

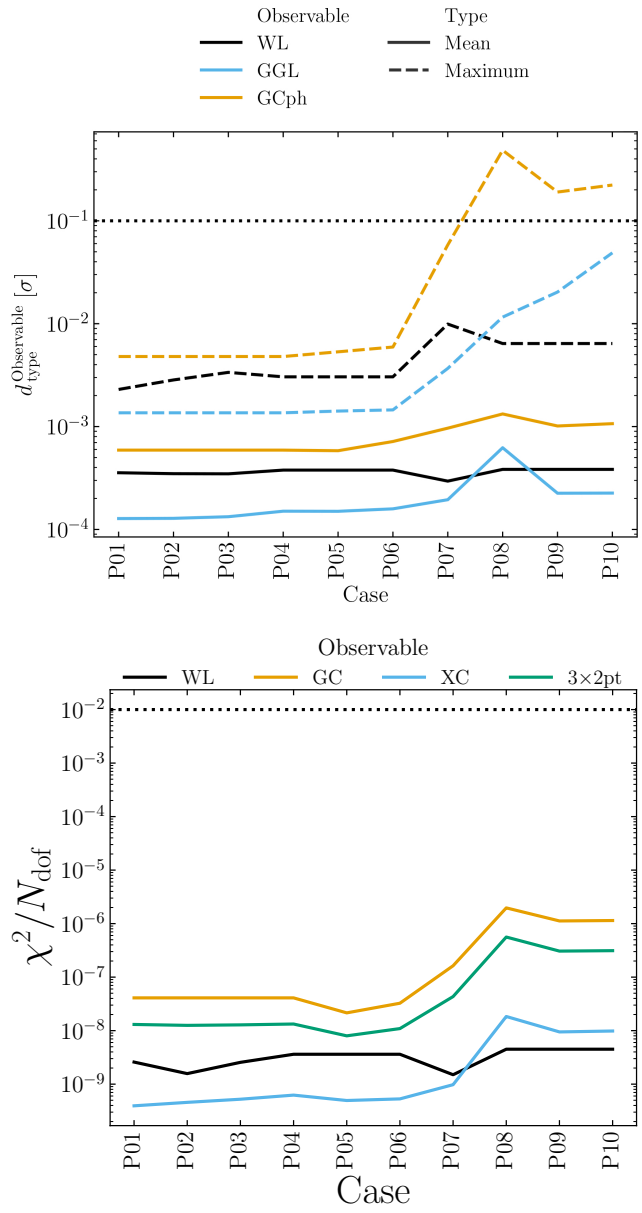

Fig. C.1. Equivalent of Fig. 2 using CCL as a benchmark.

These basic cosmological ingredients necessary for CLOE are:

- the normalised Hubble rate $E(z) \equiv H(z)/H_0$;
- the comoving distance $r(z)$;
- the linear matter power spectrum $P_{\rm m}^{\rm LIN}(k, z)$.

Through these functions, CLOE computes other derived cosmological quantities, such as the growth factor $g_+(z)$ and the growth rate $f(z)$, and later combines them all to compute the observables (for details, see Paper 1). While the linear matter power spectrum $P_{\delta\delta}^{\rm LIN}$ is not used directly in any calculation, this is the input for the non-linear methods used in CLOE, and therefore it constitutes one of the relevant cosmological quantities.

In Fig. D.1, we show the SMAPE obtained for these four main functions, with the comparison for the last function performed at four different values of the redshift.

We find no significant difference in these functions when switching between the two Boltzmann solvers, with all the differences being at most at the level of one per cent. Such a result is not surprising, given that the structure choices made in developing CLOE were also aimed at removing any dependence on the choice of the solver. Nevertheless, the results found highlight how, also in the part of the code that directly interfaces with the Boltzmann solvers, the differences are not significant.

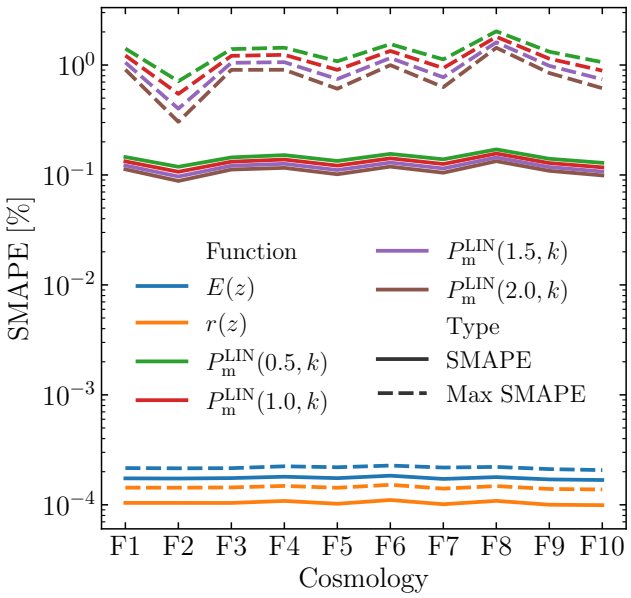

Fig. D.1. Summary SMAPE values for the comparison between the cosmological function extracted from the Boltzmann solver in the CLOE +CAMB and CLOE +CLASS configurations.